

Interplay of Phase II Enzymes and Transporters in Futile Cycling:  
Influence of Mrp2-Mediated Excretion of Estradiol 17 $\beta$  D-Glucuronide and Its 3-Sulfate  
Metabolite on Net Sulfation in Perfused TR<sup>-</sup> and Wistar Rat Liver Preparations

Huadong Sun<sup>1</sup>, Ying-Ying Zeng, and K. Sandy Pang

Department of Pharmaceutical Sciences (H.S., Y. Z., K.S.P.), Leslie Dan Faculty of Pharmacy,  
and Department of Pharmacology (K.S.P.), Faculty of Medicine,  
University of Toronto, Toronto, Canada M5S 3M2

## Running Title Page

Running Title: Transporter-enzyme interplay in futile cycling

Correspondence Author: Dr. K.S. Pang  
Leslie Dan Faculty of Pharmacy  
University of Toronto  
144 College Street  
Toronto, ON M5S 3M2 Canada  
Tel: 416-978-6164  
Fax: 416-978-8511  
E-mail: ks.pang@utoronto.ca

Text: 26 pages

Tables: 4

Figures: 6

References: 39

Abstract: 250 words

Introduction: 721 words

Discussion: 1369 words

Appendix: 2 pages

Abbreviations: E<sub>2</sub>17G, estradiol 17 $\beta$  D-glucuronide; E<sub>2</sub>3S17G, estradiol 3-sulfate-17 $\beta$  D-glucuronide; 4-MUS, 4-methylumbelliferyl sulfate; Sult1e1, estrogen sulfotransferase; Oatp, organic anion transporting polypeptide; Mrp, multidrug resistance-associated protein; AUC, area under the concentration-time curve; PBPK model, physiological-based pharmacokinetic model.

## ABSTRACT

The hepatic disposition of estradiol 17 $\beta$  D-glucuronide (E<sub>2</sub>17G), a substrate of the Oatp's (Oatp1a1, Oatp1a4, Oatp1b2), was investigated in Wistar and TR<sup>-</sup> (Mrp2-mutant) rats to elucidate how absence of Mrp2, the major excretory transporter for both E<sub>2</sub>17G and its 3-sulfate metabolite (E<sub>2</sub>3S17G), affected the net sulfation. With absence of Mrp2, lower microsomal desulfation activity and higher Mrp3 but unchanged, immunoreactive protein expression of other transporters (Oatp's and Mrp4) and estrogen sulfotransferase (Sult1e1) were found in TR<sup>-</sup> rats. In recirculating, perfused liver preparations, the rapid decay of E<sub>2</sub>17G and sluggish appearance of low levels of E<sub>2</sub>3S17G in perfusate for Wistar livers were replaced by a protracted, bi-exponential decay of E<sub>2</sub>17G and greater accumulation of E<sub>2</sub>3S17G, whose levels reached plateaus upon the almost complete obliteration of biliary excretion of E<sub>2</sub>17G and E<sub>2</sub>3S17G in the TR<sup>-</sup> liver. Much higher amounts of E<sub>2</sub>17G (28x) and E<sub>2</sub>3S17G (11x) in liver and reduced net sulfation (40% $\pm$ 6% from 77% $\pm$ 6% dose,  $P$  < 0.05) were observed at 2 h for the TR<sup>-</sup> vs. the Wistar rats. With use of a PBPK model, analytical solutions for the area under the curves (AUCs) for the precursor and metabolite were obtained to reveal how enzyme- and transporter-mediated processes affected the hepatic disposition of the precursor and metabolite in futile cycling. The analytical solutions were useful to explain transporter-enzyme interplay in futile cycling and predicted that a shutdown of Mrp2 function led to decreased net sulfation of E<sub>2</sub>17G by raising the intracellular concentration of the metabolite, E<sub>2</sub>3S17G, which readily refurnished E<sub>2</sub>17G via desulfation.

## INTRODUCTION

The liver is the most important drug eliminatory organ and involves enzymes and basolateral influx/efflux and canalicular transporters for entry and elimination. The basolateral influx transporters (organic anion transporting polypeptides, Oatp's, sodium-dependent taurocholate co-transporting polypeptide, organic anion transporter 2, and organic cation transporter 1) regulate the entry of substrate into the cell to undergo metabolism by Phase I and/or Phase II enzymes. Then both the parent drug and Phase II metabolites are subject to canalicular transport via the P-glycoprotein, multidrug resistance-associated protein 2 (MRP2), bile salt export pump, and the breast cancer resistance protein, whereas basolateral efflux occurs via MRP3 and MRP4 into sinusoidal blood. Although metabolism is normally deemed as irreversible, the metabolite, on occasion, may re-form the parent drug. This phenomenon, known as “reversible metabolism” or “futile cycling”, describes the interconversion between the parent drug and its metabolite. This can occur between a precursor and its phase I (Meffin et al., 1983; Baillie et al., 2001) or phase II (Hansen and Morris, 1996; Grubb et al., 1999) metabolites. For example, the sulfated metabolite formed via sulfotransferases (SULT's) in the cytosol may access the arylsulfatases in the endoplasmic reticulum to become desulfated to re-form the parent drug (Ratna et al., 1993; Kauffman et al., 1998). Acinar heterogeneity of the SULT's further complicates the scenario (Xu et al., 1993; Tan et al., 2001).

A well-stirred liver model with membrane barriers has been shown useful to relate the physiological and biochemical factors to hepatic drug and metabolite processing (Sirianni and Pang, 1997, Liu and Pang, 2005, Sun and Pang, 2010). Briefly, transporter or enzyme activity is denoted by the intrinsic clearance, or the ratio of  $V_{\max}$  and  $K_m$  under linear conditions. The  $CL_{in}$  and  $CL_{ef}$  relate to the summed transport activities due to the influx and efflux transporters and

passive diffusion, respectively, at the basolateral membrane;  $CL_{int,met}$  is the enzymatic metabolic activity and  $CL_{int,sec}$  is the canalicular, secretory transporter activity. Solutions for the apparent total liver, metabolic, and excretory clearances ( $CL_{liver,total}$ ,  $CL_{liver,met}$  and  $CL_{liver,ex}$ , respectively) for a drug that is metabolized irreversibly had revealed that all these transport and metabolic intrinsic clearances modulate the apparent clearances of alternate pathways. The  $CL_{liver,met}$  is dependent not only on  $CL_{int,met}$  but also on  $CL_{int,sec}$ . Similarly,  $CL_{int,met}$  appears in the solution of  $CL_{liver,ex}$ . Accordingly, the interplay between enzymes and canalicular efflux transporters was described as a “see-saw” phenomenon (Sirianni and Pang, 1997; Liu and Pang, 2005), since both enzymes and canalicular efflux transporters would compete for the intracellular substrate. An increase of  $CL_{int,sec}$  would lead to an increase in the  $CL_{liver,ex}$  and  $CL_{liver,total}$  but would result in decreased  $CL_{liver,met}$ , the compensatory pathway of drug elimination. The opposite trend would arise when  $CL_{int,sec}$  is decreased. Analogous changes of the apparent clearances would result with changes in  $CL_{int,met}$  (Liu and Pang, 2005). However, the transporter-enzyme interplay in the presence of futile cycling remains unknown.

Transporter or enzyme activity can be perturbed with use of a specific inhibitor or inducer and knockout or knockdown of the target gene, whereby the resultant changes in drug processing can be evaluated. The Groningen Yellow/transporter-deficient ( $TR^-$ ) rats are derived from Wistar rats but lack the functional Mrp2 due to a single nucleotide substitution in the Mrp2 gene (Jansen et al., 1985; Müller et al., 1996; Ito et al., 1997). This renders the  $TR^-$  rat as a useful animal model to assess the role of Mrp2 in drug biliary excretion as well as the interplay of Mrp2 and other transporters and enzymes (Xiong et al., 2000). In this communication, the effect of Mrp2 on net sulfation and futile cycling of estradiol 17 $\beta$  D-glucuronide ( $E_217G$ ) and its 3-sulfated metabolite ( $E_23S17G$ ) was assessed by comparison of their disposition in recirculating, perfused the  $TR^-$

(lacking Mrp2) and Wistar rat liver preparations. In the rat liver, E<sub>2</sub>17G is taken up efficiently by Oatp1a1, Oatp1a4, and Oatp1b2 at the basolateral membrane (Cattori et al., 2001). In rat hepatocytes, E<sub>2</sub>17G is sulfated mainly by the estrogen sulfotransferase (Sult1e1) to form E<sub>2</sub>3S17G, which is desulfated back to re-form E<sub>2</sub>17G by arylsulfatase C (Sun et al., 2006); both E<sub>2</sub>17G and E<sub>2</sub>3S17G are secreted into bile, predominantly via Mrp2 (Morikawa et al., 2000). Mrp3 and Mrp4 are expressed at low levels under physiological conditions, and when up-regulated, would play an important role by enhancing the efflux of E<sub>2</sub>17G and E<sub>2</sub>3S17G back to the blood.

## MATERIALS AND METHODS

### Materials and animals

[6,7-<sup>3</sup>H]E<sub>2</sub>17G (specific activity 46.9 Ci/mmol) was purchased from Perkin Elmer Life Sciences Inc. (Boston, MA). [6,7-<sup>3</sup>H]E<sub>2</sub>3S17G was biosynthesized by recirculation of [6,7-<sup>3</sup>H]E<sub>2</sub>17G (~ 100,000 dpm/ml) in blood perfusate at 12 ml/min through the rat liver. The bile was pooled and lyophilized, then reconstituted and injected into HPLC (see HPLC methods); the eluant fractions corresponding to [6,7-<sup>3</sup>H]E<sub>2</sub>3S17G (retention time 12-13 min) were pooled and desalted by reverse phase Sep-Pak cartridge (Waters, MA), and the purified content was concentrated and stored at - 20°C. The radiochemical purities of [6,7-<sup>3</sup>H]E<sub>2</sub>17G and [6,7-<sup>3</sup>H]E<sub>2</sub>3S17G were measured by HPLC as 98% and 97%, respectively. Unlabeled E<sub>2</sub>17G, 4-methylumbelliferyl sulfate (4-MUS), and bovine serum albumin in Tyrode's solution were obtained from Sigma Aldrich Canada (Mississauga, ON). Dextrose 50% USP injection was obtained from Abbott Laboratories (Montreal, QC) and Dextran T-40 was purchased from GE Health Care (Uppsala, Sweden). Antibodies for Oatp1a1 and Oatp1a4 were kind gifts from Dr. Allan W. Wolkoff (Albert Einstein College of Medicine, Bronx, NY); the antibody for Oatp1b2 was kindly provided by Dr. Richard B. Kim (University of Western Ontario, London, Ontario, Canada). The Sult1a1 antibody was donated by Dr. Charles N. Falany (University of Alabama at Birmingham, Birmingham, AL), and Sult1e1 monoclonal antibody was purchased from Abcam (Cambridge, MA). The Mrp2 antibody (M2III-6) was obtained from AXXORA, LLC (San Diego, CA); the Mrp3 and Mrp4 antibodies were generously provided by Dr. Yuichi Sugiyama (University of Tokyo, Tokyo, Japan) and Dr. John D. Schuetz (St. Jude Children's Research Hospital, Memphis, TN), respectively. All other reagents were of HPLC grade, and de-ionized distilled water was used in all experiments.

Male Wistar rats were purchased from Charles River (St. Constant, QC, Canada). TR<sup>-</sup> rats were generously provided by Dr. Kim L.R. Brouwer (University of North Carolina at Chapel Hill, NC) and bred in the Division of Comparative Medicine, University of Toronto. All the rats were maintained under a 12:12-h dark-light cycle in the housing facility (two rats/cage) and given access to animal chow and water *ad libitum*. The procedures used for the animal studies were conducted in accordance with the protocols approved by Animal Committee at the University of Toronto.

### **Analytical solutions of area under the concentration-time curve (AUCs) and cumulative biliary excretion (from time=0 to infinity, $A_{e,\infty}$ )**

A physiologically based pharmacokinetic (PBPK) model (Fig. 1) was used to describe the transport and metabolism of a precursor and metabolite pair that undergoes futile cycling. The model consists of the reservoir, sinusoid, hepatocyte, and bile compartments, denoted by subscripts R, LB, L, and bile, respectively. D and Mi represent the precursor and the interconversion metabolite, respectively. The precursor ( $D_R$ ) and metabolite ( $Mi_R$ ) in the reservoir are delivered at a flow rate of  $Q_L$  (12 ml/min) to the liver. The concentrations of drug ( $D_{LB}$ ) and metabolite ( $M_{LB}$ ) in sinusoidal blood are identical to those in the reservoir. The unbound fractions that describe the binding of the precursor and metabolite in sinusoidal blood are denoted by  $f_{LB}$  and  $f_{LB\{mi\}}$ , respectively, and are identical to those in perfusate blood,  $f_B$  and  $f_{B\{mi\}}$ , respectively. The unbound fractions in the liver for the precursor and metabolite are denoted by  $f_L$  and  $f_{L\{mi\}}$ , respectively. The unbound precursor and metabolite in sinusoid that rapidly equilibrate with the species bound to albumin ( $D_{LB-BSA}$ ,  $Mi_{LB-BSA}$ ) and red blood cells ( $D_{LB-rbc}$ ,  $Mi_{LB-rbc}$ ), are taken up into the hepatocyte with the influx clearances,  $CL_{in}$  and  $CL_{in\{mi\}}$ , respectively.

Within the hepatocyte, the precursor drug is metabolized to its interconversion metabolite with the metabolic intrinsic clearance,  $CL_{int,met}^{D \rightarrow Mi}$ , and to other metabolites with the metabolic intrinsic clearance,  $CL_{int,met}^{other}$ . Likewise, the metabolite re-forms the precursor drug with the metabolic intrinsic clearance of the metabolite,  $CL_{int,met}^{Mi \rightarrow D}\{mi\}$ , or forms other secondary metabolites with the intrinsic clearance,  $CL_{int,met}^{other}\{mi\}$ . Both the precursor and metabolite in the hepatocyte may be effluxed back to the sinusoid with  $CL_{ef}$  and  $CL_{ef}\{mi\}$ , respectively, or excreted into bile with  $CL_{int,sec}$  and  $CL_{int,sec}\{mi\}$ , respectively. The bile flow rate is  $Q_{bile}$ .

The AUCs ( $AUC_R$  and  $AUC_L$ ) and cumulative biliary excretion of drug and metabolite were solved analytically by the inversion of matrices derived for the model (Fig. 1) and the associated mass balance equations, shown in the Appendix, with the computer software, Maple™ (Maple Inc., Waterloo, ON). In absence of futile cycling, other parameters were kept the same except that  $CL_{int,met}^{Mi \rightarrow D}\{mi\}$  was set to 0.

### Preparation of subcellular fractions

Rat livers at the end of perfusion were used for the preparation of crude membranes and cytosolic fractions for immunoblotting. As described previously (Sun et al., 2006), the liver tissue was homogenized in buffer (250 mM sucrose, 10 mM HEPES, 10 mM Tris-base, pH 7.4), and centrifuged at 3,000 g for 10 min; the resultant supernatant was centrifuged at 33,000g for 1 h. The pellet (crude membrane) was reconstituted in resuspension buffer (mannitol 50 mM, 20 mM HEPES, in 20 mM Tris-base, pH 7.5). For preparation of the cytosolic fraction, the liver tissue was homogenized in SET buffer (250 mM sucrose, 1 mM EDTA, 10 mM Tris-HCl, pH 7.4). The homogenate was centrifuged at 3,000 g for 20 min and the resultant supernatant was further centrifuged at 100,000 g for 1 h to yield the microsomal and cytosolic fractions that were used for

Western blotting. All buffers were freshly prepared and supplemented with protease inhibitor cocktail (Sigma, Oakville, ON). The microsomal fraction prepared as follows, was used for the assay of sulfatase activities. A piece of liver tissue was homogenized with Tris-HCl (25 mM, pH 7.4). The homogenate was centrifuged at 9,000 g for 20 min. The resultant supernatant (S9) was centrifuged at 100,000 g for 1 h; the pellet was resuspended in Tris-HCl (25 mM, pH 7.4) to yield the microsomal fraction. All of the procedures were carried out at 4°C, and subcellular fractions were stored at -80 °C until analyses. Protein concentration was determined by the Lowry method (Lowry et al., 1951).

### **Immunoblot analysis**

Protein expression of the Oatp's, Mrp's and Sult's in the perfused rat livers was determined semi-quantitatively by immunoblotting. In brief, 20 µg of crude membrane (for Oatp's and Mrp's) or cytosolic (for Sult's) proteins were resolved by SDS-PAGE in 7.5% (for Mrp's), 10% (for Oatp's), and 12% (for Sult's) gels, and electrophoretically transferred onto nitrocellulose membranes. The blots were blocked with TBS-T (1%) buffer containing 5% nonfat milk for 15 min, then incubated with primary antibodies (rabbit-anti-Oatp1a1 at 1:2500, rabbit-anti-Oatp1a4 at 1:10000, rabbit-anti-Oatp1b2 at 1:5000, mouse-anti-Mrp2 at 1:750, rabbit-anti-Mrp3 at 1:5000, rabbit-anti-Mrp4 at 1:2000, rabbit-anti-Sult1a1 and mouse-anti-Sult1e1 at 1:10,000) overnight at 4°C. Finally, goat-anti-rabbit (for Oatp's, Mrp3, Mrp4, Sult1a1) or goat-anti-mouse (for Sult1e1 and Mrp2) IgG (H+L)-HRP conjugate (Bio-Rad Laboratories, Hercules, CA) was incubated with the blots at room temperature for 1 h. Upon reaction with ECL, the blots were scanned by FluorChem<sup>TM</sup> Imaging System (Alpha Innotech, San Leandro, CA) and the scan time was controlled to ensure linearity of the chemiluminescent signal. The autoradiograms obtained were quantified densitometrically with Scion Image (Scion Corporation, Frederick, MD). Since the

MWs of Oatp's and Mrp's (> 75 kD) are distinctly different from that of GAPDH (~ 37 kD), the loading control, the blot was cut into two portions after transfer: the upper portion was used for the detection of the target protein, and the lower portion was used for the detection of GAPDH. Since the Sult's have similar MWs as GAPDH, the blot was stripped with the restore western blot stripping buffer (Pierce Biotechnology Inc., Rockford, IL) and re-probed with the antibody for GAPDH (Abcam Inc., Cambridge, MA), after the target protein was quantified. Protein expression of the target protein was presented as the ratio of densitometric measurements of the target protein to that of GAPDH.

### **In vitro sulfatase activity in subcellular fractions**

As described previously (Sun et al., 2006), a relatively higher microsomal protein concentration (4 mg/ml) was used for the incubation study due to the low sulfatase activity towards E<sub>2</sub>3G17G. [<sup>3</sup>H]E<sub>2</sub>3S17G (~ 50,000 dpm) and Tris-HCl (25 mM, pH 7.4) were separately pre-incubated at 37 °C for 5 min and then mixed (1:1, v/v) and incubated in a rotating incubator at 37°C for 10 min. Samples were retrieved at various times between 0 and 10 min to determine the time-linearity in [<sup>3</sup>H]E<sub>2</sub>17G formation. The reaction was terminated by the addition of 150 µl ice-cold acetonitrile that contained 4-MUS (50 µg/ml) as an internal standard. After centrifugation at 6000 g for 10 min, the resultant supernatant was dried under a gentle stream of nitrogen. The residue was reconstituted in the buffer (NH<sub>4</sub>Ac: acetonitrile = 85:15, v/v) and the resultant sample was subjected to HPLC (see below). The radioactivities in outflow eluants that corresponded to peaks of the radiochromatogram were collected. A calibration curve was constructed by mixing boiled microsomal fractions with the varying known concentrations of [<sup>3</sup>H]E<sub>2</sub>17G for the quantification of the [<sup>3</sup>H]E<sub>2</sub>17G formed in microsomes. The in vitro, desulfation intrinsic clearance ( $CL_{int,met}^{Mi \rightarrow D}$  {mi}<sub>in vitro</sub> in µl/s/mg microsomal protein), estimated as the formation rate of

[<sup>3</sup>H]E<sub>2</sub>17G divided by the concentration of [<sup>3</sup>H]E<sub>2</sub>3S17G, was only an apparent value since the estimate did not consider the binding of E<sub>2</sub>3S17G to microsomal proteins.

### **Recirculating rat liver perfusion**

The surgical procedure and the perfusion apparatus were described previously (Sun et al., 2006). In brief, the male Wistar or TR<sup>-</sup> rat serving as liver donors was anesthetized by an intraperitoneal injection of a mixture of ketamine (90 mg/kg) and xylazine (10 mg/kg). Cannulae were placed in the portal vein, hepatic vein, and bile duct, and the temperature of the liver preparation was maintained close to be 37 °C under a heating lamp. Blank perfusate was oxygenated (95% O<sub>2</sub>-5% CO<sub>2</sub>) Krebs Henseleit bicarbonate solution (pH 7.4) that was supplemented with washed bovine erythrocytes (~20%) (a kind gift of Ryding-Regency Meat Packers Ltd., Toronto, ON, Canada), 1% bovine serum albumin, 3% Dextran T-40 and 0.3% glucose. Reservoir perfusate containing [<sup>3</sup>H]E<sub>2</sub>17G (~ 100,000 dpm/ml) was prepared by mixing trace amounts of [<sup>3</sup>H]E<sub>2</sub>17G (~ 45 nM) with perfusate in the reservoir. Perfusate was delivered at 12 ml/min to TR<sup>-</sup> (13.7 ± 0.9 g, n = 4) or Wistar (13.7 ± 2.3 g, n = 4) rat livers via the portal vein cannula and allowed to exit via the hepatic vein cannula to return to the reservoir. The rat liver preparation was initially perfused by blank perfusate for 20 min for equilibration at 37 °C. Thereafter, the blood supply was switched to the alternate reservoir containing the [<sup>3</sup>H]E<sub>2</sub>17G in the perfusate. Perfusate in reservoir was sampled at 0, 2.5, 7.5, 12.5, 17.5, 22.5, 27.5, 35, 45, 55, 70, 90, and 110 min, and bile was collected at 5 min intervals up to 30 min, and subsequently at 10 or 20 min intervals until 120 min. At the end of the experiment (120 min), the liver was flushed with 50 ml ice-cold KHB, carefully excised, blotted with gauze and weighed. Then the liver tissue was minced, snap-frozen with liquid nitrogen, and stored at -80°C. The perfusate and bile samples were kept at -20 °C until analyses.

## HPLC methods

A Shimadzu HPLC system consisting of a C<sub>18</sub> reverse-phase column (Alltech Associates, Deerfield, IL; 4.6 x 250 mm, particle size, 10  $\mu$ m), a guard column (Waters Bondapak C18/Corasil 37–55  $\mu$ m), and a Shimadzu 10A apparatus, was used for the separation of E<sub>2</sub>17G and E<sub>2</sub>3S17G at 280 nm. A binary HPLC gradient program (A, 10 mM ammonium acetate, pH 5.0, adjusted with 10% acetic acid; B, acetonitrile) was used (Sun et al., 2006). HPLC elution was initiated at 15% B at the flow rate of 1 ml/min, maintained for 13 min, followed by a linear increase of %B to 22% and to the flow rate to 1.2 ml/min within the next min, and was maintained there until 24 min. The %B was linearly increased to 50% over the next min, and maintained for another 10 min. Then the flow rate and %B were returned to the initial conditions over 1 min and maintained for another 5 min.

**Perfusate samples.** Blood perfusate samples (100-500  $\mu$ l) were made up to 500  $\mu$ l with blank perfusate, and deproteinized with 2 ml of methanol, as described previously (Sun et al., 2006). After 5 min centrifugation at 1500 g, 2 ml of the supernatant was mixed with 8 ml Ready Safe scintillation cocktail (Beckman Coulter Canada) and counted. A calibration curve was prepared in identical fashion to quantify the total radioactivity in perfusate sample. Then the dpm's of [<sup>3</sup>H]E<sub>2</sub>17G and [<sup>3</sup>H]E<sub>2</sub>3S17G in the sample were determined. Each perfusate sample was added 2 ml of acetonitrile (1:4, v/v), mixed for 10 sec, and centrifuged at 1500 g for 5 min to precipitate the protein. The resultant supernatant was extracted with toluene (1:1, v/v) to remove the acetonitrile, and the remaining water layer was injected directly into the HPLC. Radioactive eluants corresponding to [<sup>3</sup>H]E<sub>2</sub>17G (retention time ~21 min) and [<sup>3</sup>H]E<sub>2</sub>3S17G (retention time ~12-13 min) were collected and counted. The [<sup>3</sup>H]E<sub>2</sub>17G and [<sup>3</sup>H]E<sub>2</sub>3S17G concentrations in each perfusate sample were obtained by multiplying the total radioactivity of each sample to the

fraction of [ $^3\text{H}$ ]E<sub>2</sub>17G and [ $^3\text{H}$ ]E<sub>2</sub>3S17G, respectively, after HPLC separation. It was noted that the radioactivity in perfusate collected beyond 45 min for the Wistar liver preparation was too low to be quantified accurately.

**Liver samples.** A piece of liver tissue was homogenized with ice-cold saline (1:4, v/v) over ice. An aliquot of 250  $\mu\text{l}$  of homogenate was mixed with 1 ml of Soluene-350 and incubated at 60  $^{\circ}\text{C}$ , with intermittent swirling. Then 0.2 ml of 30% hydrogen peroxide was added and incubated for 5 min at room temperature, followed by the addition of another 0.2 ml of 30% hydrogen peroxide for another 10 min of incubation at room temperature. The resultant solution was then incubated at 60  $^{\circ}\text{C}$  for 30 min. Thereafter the addition of 10 ml of Hionic-Fluor cocktail, the final solution was counted to obtain the total radioactivity in the liver tissue sample. For determination of the fraction of [ $^3\text{H}$ ]E<sub>2</sub>17G and [ $^3\text{H}$ ]E<sub>2</sub>3S17G in liver tissue, 100  $\mu\text{l}$  TR<sup>-</sup> liver homogenate or 500  $\mu\text{l}$  Wistar liver homogenate was spiked with 50  $\mu\text{l}$  4-MUS (50  $\mu\text{g}/\text{ml}$ , internal standard) and 1.5 ml acetonitrile, then mixed for 10 sec and centrifuged at 3,000 g for 5 min. The supernatant (1.8 ml) was extracted against an equal volume of toluene; the resultant, bottom (water) layer was used for injection into the HPLC. Calibration curves were prepared by admixing varying concentrations of [ $^3\text{H}$ ]E<sub>2</sub>17G or [ $^3\text{H}$ ]E<sub>2</sub>3S17G with boiled liver homogenate fractions obtained from TR<sup>-</sup> and Wistar livers. Standards of the calibration curve for the liver samples were processed in parallel under identical conditions. [ $^3\text{H}$ ]E<sub>2</sub>17G and [ $^3\text{H}$ ]E<sub>2</sub>3S17G in liver samples were quantified by the ratio of the corresponding radioactivities to the chromatographic area of 4-MUS, with use of each individual calibration curve. The concentrations of [ $^3\text{H}$ ]E<sub>2</sub>17G and [ $^3\text{H}$ ]E<sub>2</sub>3S17G in the liver tissue were calculated by multiplying the total radioactivity to the fraction of [ $^3\text{H}$ ]E<sub>2</sub>17G and [ $^3\text{H}$ ]E<sub>2</sub>3S17G, respectively.

**Bile samples.** Each bile sample was diluted with 300  $\mu$ l H<sub>2</sub>O. An aliquot of the diluted bile sample was counted directly for the total radioactivity, and another aliquot was injected into the HPLC. The [<sup>3</sup>H]E<sub>2</sub>17G and [<sup>3</sup>H]E<sub>2</sub>3S17G radioactivities in the eluant fractions were counted to determine the fractions of [<sup>3</sup>H]E<sub>2</sub>17G and [<sup>3</sup>H]E<sub>2</sub>3S17G in each sample, and these were multiplied to the total dpm to provide the dpm of [<sup>3</sup>H]E<sub>2</sub>17G and [<sup>3</sup>H]E<sub>2</sub>3S17G in the sample.

### PBPK Modeling and Simulation

Since E<sub>2</sub>17G and E<sub>2</sub>3S17G accounted for more than 98% radioactivity in the system, the other metabolic pathways for E<sub>2</sub>17G and E<sub>2</sub>3S17G,  $CL_{int,met}^{other}$  and  $CL_{int,met}^{other}\{mi\}$ , respectively, were set to be zero in the PBPK model (Fig. 1). The mass balance equations for this model are shown in the Appendix.

The PBPK model was also used for fitting and simulations. Inasmuch the model for futile cycling was extremely complicated, the likelihood of success for data fitting was low. As alternate measures, simulations were used. Various assumptions, highlighted in the Results Section, were taken for parameter estimates. The influx clearances for E<sub>2</sub>17G and E<sub>2</sub>3S17G were taken to be the same as that of Sun et al. (2006). Additionally, the attainment of steady-state conditions for E<sub>2</sub>17G and E<sub>2</sub>3S17G in the TR<sup>-</sup> rat allowed estimation of  $CL_{in}$ ,  $CL_{ef}$ ,  $CL_{in}\{mi\}$ ,  $CL_{ef}\{mi\}$ , and the sulfation and desulfation intrinsic clearances, as described later in the Results Section. It was further assumed that the unbound fractions  $f_L$ ,  $f_B\{mi\}$ , and  $f_L\{mi\}$  equaled that observed  $f_B$  (Sun et al., 2006).

Parameter estimates of the interconversion and secretory intrinsic clearances for the Wistar rat were obtained from fitting upon fixing the values of  $CL_{in}$ ,  $CL_{ef}$ ,  $CL_{in}\{mi\}$ , and  $CL_{ef}\{mi\}$ . The relative intensities of the immunoblots obtained from Wistar and TR<sup>-</sup> livers were then compared to provide estimates of relative transporter activities for all sinusoidal influx (Oatp's), basolateral

efflux (Mrp3), and for the relative sulfation (Sult1e1) activities, keeping in mind that the ex vivo desulfation activity could be obtained by scale-up of the in vitro microsomal activity. These optimized values were used for simulation of the concentrations/amounts of E<sub>2</sub>17G and E<sub>2</sub>3S17G in perfusate, liver, and bile according to the differential equations shown in the Appendix. The estimates were also used to simulate the AUCs and clearances with various extents of reduction of Mrp2 activity.

### **Statistical analyses**

The data were presented with mean values  $\pm$  SD. The two-tail Student's *t* test was used to compare the means, and a *P* value of  $< 0.05$  was viewed as significant.

## RESULTS

### Solved analytical solution for AUC and $A_{e,\infty}$

As shown in Table 1, the solutions for  $AUC_R$  and  $AUC_R\{mi,P\}$  were similar to those in the absence of futile cycling (de Lannoy et al., 1993; Sirianni and Pang, 1997), with the exception that the  $ef_m''$  and  $ef_m'$  terms are now present. Both terms,  $ef_m''$  and  $ef_m'$ , were introduced to describe modulation of the backward and forward processes in futile cycling, respectively, on the net metabolism of the precursor and metabolite. In these solutions,  $ef_m''$  or effective coefficient for metabolite formation, was associated with  $CL_{int,met}^{D \rightarrow Mi}$  or the metabolite formation intrinsic clearance. The term  $ef_m''$  or  $\frac{CL_{int,sec}\{mi\} + CL_{int,met}^{other}\{mi\}}{CL_{int,sec}\{mi\} + CL_{int,met}^{Mi \rightarrow D}\{mi\} + CL_{int,met}^{other}\{mi\}}$  consisted of intrinsic clearance terms associated with the metabolite: the intrinsic clearance denoting re-formation of the precursor  $CL_{int,met}^{Mi \rightarrow D}\{mi\}$  as well as other terms for secretion ( $CL_{int,sec}\{mi\}$ ) and sequential metabolism ( $CL_{int,met}^{other}\{mi\}$ ) of the metabolite. Conversely,  $ef_m'$  or the effective recycling coefficient,  $\frac{CL_{int,sec} + CL_{int,met}^{other}}{CL_{int,sec} + CL_{int,met}^{D \rightarrow Mi} + CL_{int,met}^{other}}$ , was associated with the metabolic intrinsic clearance of metabolite to re-form the precursor,  $CL_{int,met}^{Mi \rightarrow D}\{mi\}$  that appeared as in the denominator of the solution of  $AUC_R\{mi,P\}$  and  $AUC_L\{mi,P\}$  in the presence of futile cycling (Table 1).

The area under the curve for the precursor in reservoir,  $AUC_R$ , was found to depend on all the intrinsic clearances of the precursor, including basolateral influx ( $CL_{in}$ ) and efflux ( $CL_{ef}$ ), metabolic ( $CL_{int,met}^{D \rightarrow Mi}$  and  $CL_{int,met}^{other}$ ) and secretory ( $CL_{int,sec}$ ) intrinsic clearances. The net metabolite formation intrinsic clearance of the precursor ( $ef_m'' CL_{int,met}^{D \rightarrow Mi}$ ) was reduced by the factor of  $(1 - ef_m'')$ , or  $\frac{CL_{int,met}^{Mi \rightarrow D}\{mi\}}{CL_{int,sec}\{mi\} + CL_{int,met}^{Mi \rightarrow D}\{mi\} + CL_{int,met}^{other}\{mi\}}$ . The area under the curve for the formed metabolite in

the reservoir,  $AUC\{mi,P\}_R$ , was found to depend on parameters relating to metabolite handling ( $CL_{in}\{mi\}$ ,  $CL_{ef}\{mi\}$ ,  $CL_{int,sec}\{mi\}$ ,  $CL_{int,met}^{Mi \rightarrow D}\{mi\}$ ) and metabolite formation ( $CL_{int,met}^{D \rightarrow Mi}$ ), and the secretory intrinsic clearance ( $CL_{int,sec}$ ), metabolic intrinsic clearance for alternate metabolism ( $CL_{int,met}^{other}$ ) and the total intrinsic clearance of the precursor ( $CL_{int,sec} + CL_{int,met}^{D \rightarrow Mi} + CL_{int,met}^{other}$ ). Analogously,  $AUC_L$  and  $AUC_L\{mi,P\}$ , and the cumulative excretion of the precursor ( $A_{e,\infty}$ ) and metabolite ( $A_{e,\infty}\{mi,P\}$ ) were modified by  $ef_m''$  or  $ef_m'$  accordingly, when futile cycling existed. The apparent total ( $CL_{liver,tot}$ ) and excretory ( $CL_{liver,ex}$ ) clearances of the liver were estimated as dose/ $AUC_R$  and  $A_{e,\infty}/AUC_R$ , respectively. The apparent metabolic clearance ( $CL_{liver,met}$ ) was obtained from the difference between  $CL_{liver,tot}$  and  $CL_{liver,ex}$  (Table 2). In absence of a membrane barrier, the basolateral uptake and efflux clearances ( $CL_{in} = CL_{ef}$ ) were set to greatly exceed  $CL_{int,sec}$ ,  $ef_m'' CL_{int,met}^{D \rightarrow Mi}$  and  $CL_{int,met}^{other}$ . As noted,  $ef_m''$ , together with  $CL_{int,met}^{D \rightarrow Mi}$ , appeared in the solutions of all the apparent clearances (Table 2).

### Relative protein expression from immunoblotting

As shown in Fig. 2, Mrp3 protein expression was significantly increased in the TR<sup>-</sup> liver compared to that in the Wistar liver ( $4.26 \pm 1.08$  vs.  $1.00 \pm 0.65$ ), and Mrp2 protein expression was absent in the TR<sup>-</sup> rat. However, protein expression of other transporters: Oatp1a1, 1a4, 1b2, and Mrp4, and enzymes (Sult1e1 and Sult1a1) were not significantly different between TR<sup>-</sup> and Wistar livers (Fig. 2).

### Desulfation activity of microsomal fractions

The apparent desulfation activity towards E<sub>2</sub>S17G in microsomal fractions prepared from TR<sup>-</sup> rat livers ( $CL_{int,met}^{Mi \rightarrow D}\{mi\}$  in vitro), estimated as rate of E<sub>2</sub>17G formation/ E<sub>2</sub>S17G concentration, was slightly but significantly lower than those from Wistar rat livers ( $0.07 \pm 0.02$  vs.  $0.11 \pm 0.02$

$\mu\text{l/s/mg}$  microsomal protein;  $n=3$ ). These represented apparent values since the binding of  $\text{E}_2\text{S17G}$  to microsomal proteins of Wistar and  $\text{TR}^-$  livers was not considered.

### **Recirculating liver perfusion**

In perfusate,  $\text{E}_2\text{17G}$  rapidly decayed monoexponentially for up to 45 min in the Wistar liver (Fig. 3A). Beyond that time, the radioactivity in perfusate was too low to be measured accurately. The metabolite,  $\text{E}_2\text{3S17G}$ , was present at very low levels ( $< 3\%$  dose) in the reservoir perfusate for Wistar livers, and no apparent trend was observed with time. Almost all the dose ( $92\% \pm 6\%$ ) was recovered in bile for the Wistar group at 2 h, with  $75 \pm 5\%$  dose as the  $\text{E}_2\text{3S17G}$  metabolite and  $17 \pm 4\%$  dose as the parent drug (Fig. 3B). Very low counts were found for the liver tissue of the Wistar rat at 2 h ( $\text{E}_2\text{17G}$  of  $1.4 \pm 0.7\%$  dose and  $\text{E}_2\text{3S17G}$  of  $2.5 \pm 2.1\%$  dose) (Table 3).

In contrast, perfusate  $\text{E}_2\text{17G}$  of the  $\text{TR}^-$  liver preparation decayed rapidly in the early time points, then the decay became protracted and finally reached a plateau after 1 h. The amount of  $\text{E}_2\text{3S17G}$  in perfusate appeared at much higher levels than that for Wistar preparation, and also reached a plateau after 1 h (Fig. 3C). The bile flow rate in the  $\text{TR}^-$  group was much lower than the Wistar group ( $2.4 \pm 0.5$  vs.  $6.3 \pm 0.7$   $\mu\text{l/min}$ ), as expected for rats lacking *Mrp2* (Jansen et al., 1985). As shown in Fig. 3D, almost no radioactivity ( $1.8 \pm 0.4\%$  dose at 2 h) was observed in the bile of the  $\text{TR}^-$  group. Both  $\text{E}_2\text{17G}$  and  $\text{E}_2\text{3S17G}$  were minimally excreted into bile, though  $\text{E}_2\text{17G}$  was present in slightly higher proportions ( $1.3 \pm 0.3\%$  dose) than  $\text{E}_2\text{3S17G}$  ( $0.4 \pm 0.1\%$  dose). Much radioactivity was trapped in the  $\text{TR}^-$  rat liver, with  $39 \pm 9\%$  dose at 2 h as  $\text{E}_2\text{17G}$  and  $28 \pm 5\%$  dose at 2 h as  $\text{E}_2\text{3S17G}$ . At 2 h, the fractional dose of  $\text{E}_2\text{3S17G}$  for the  $\text{TR}^-$  group was significantly lower than that in the Wistar group ( $40 \pm 6\%$  vs.  $77 \pm 6\%$ ) (Table 3).

## PBPK modeling and simulations

The volume of the reservoir ( $V_R$ ) was taken as the average value between the initial volume (200 ml) and the volume obtained at the end of the experiment, yielding values of 182 and 180 ml for the Wistar and TR<sup>-</sup> livers, respectively (Table 4). As shown in Appendix, the  $f_B$  value of E<sub>2</sub>17G was calculated from hematocrit of the perfusate, unbound fractions in plasma ( $f_p$ ), and the drug partitioning coefficient between red cells and plasma, the latter two were obtained in previous binding experiments (Sun et al., 2006). Recognizing that it was difficult to accurately determine the unbound fractions in liver tissue ( $f_L$  and  $f_{L\{mi\}}$ ) due to the presence of metabolism during incubation studies, we further assumed that unbound fractions were all equal ( $f_B = f_L = f_{B\{mi\}} = f_{L\{mi\}}$ ) for the sake of simplicity. The unbound fractions in liver would not materially alter the AUCs or clearances (Tables 1 and 2), and the value of the unbound fraction would not greatly affect the clearance of highly cleared drugs.

Since E<sub>2</sub>17G and E<sub>2</sub>3S17G levels reached a plateau 1 h after onset of perfusion among the TR<sup>-</sup> livers (Fig. 3C), rates of change for the precursor and metabolite became zero at steady state, and the left sides of all the equations in the appendix were zero. This condition allowed simplification and estimation of various parameters. At steady state, it was deduced in Eq. A3 of the Appendix that the ratio of the observed drug concentrations in perfusate and in liver ( $D_R/D_{LB}$  or 0.011) equaled the ratio of the net efflux to influx clearances since the drug concentration in reservoir equaled drug concentration in liver blood (see Eq. A1),

$$D_R/D_L = (f_L CL_{ef})/(f_B CL_{in}) = 0.011 \quad (1)$$

Analogously, Eq. A2 of the Appendix revealed that the concentration of E<sub>2</sub>3S17G in reservoir,  $Mi_R$  equaled the concentration of E<sub>2</sub>3S17G in sinusoidal blood,  $Mi_{LB}$ . It was further deduced from Eq. A4 that the ratio of the observed metabolite concentrations in perfusate and in liver ( $Mi_R/Mi_L$

= 0.02) at steady state equaled the ratio of the net basolateral efflux to influx clearances of the metabolite.

$$M_{IR}/M_{IL} = (f_L\{mi\}CL_{ef}\{mi\}) / (f_B\{mi\}CL_{in}\{mi\}) = 0.02 \quad (2)$$

From Eq. A5 or A6, it was further shown that, at steady state, the ratio of the observed metabolite to drug concentration in liver ( $M_{IL}/D_L$ ) equaled the ratio of the effective sulfation intrinsic clearance ( $f_L CL_{int,met}^{D \rightarrow Mi}$ ) to the effective desulfation intrinsic clearance ( $f_L\{mi\}CL_{int,met}^{Mi \rightarrow D}\{mi\}$ ).

$$M_{IL}/D_L = (f_L CL_{int,met}^{D \rightarrow Mi}) / (f_L\{mi\}CL_{int,met}^{Mi \rightarrow D}\{mi\}) = 0.72 \quad (3)$$

**Parameter estimates for  $CL_{in}$ ,  $CL_{ef}$ ,  $CL_{in}\{mi\}$  and  $CL_{ef}\{mi\}$ .** Since no significant difference was observed for Oatp's protein expression between the TR<sup>-</sup> and Wistar groups based on results from immunoblotting (Fig. 2), the published value of  $CL_{in}$  for E<sub>2</sub>17G (546 ml/min) of Sun et al. (2006) was assumed to hold here for both the Wistar and TR<sup>-</sup> livers. When influx is fast in relation to the flow rate, any anticipated error due to strain differences is anticipated to be inconsequential and would not affect E<sub>2</sub>17G disposition significantly (Sun et al., 2006). The value of  $CL_{in}\{mi\}$  is expected to be high since 80% of the total radioactivity of E<sub>2</sub>3S17G was rapidly secreted in bile within 15 min after intravenous dosing of [<sup>3</sup>H]E<sub>2</sub>3S17G (Slikker et al., 1983). Simulations conducted with low values of  $CL_{in}\{mi\}$  resulted in poor prediction of the data (results not shown). Thus a value similar to that of E<sub>2</sub>17G (546 ml/min) was assumed for  $CL_{in}\{mi\}$  (Table 4). From Eqs. 1 and 2, values of 5.75 and 10.9 ml/min, respectively, were calculated for  $CL_{ef}$  and  $CL_{ef}\{mi\}$  in the TR<sup>-</sup> liver. Since the Mrp3 protein expression of the TR<sup>-</sup> liver was 4.26-fold that of the Wistar liver, values for  $CL_{ef}$  and  $CL_{ef}\{mi\}$  for the Wistar liver were estimated to be 1.35 and 2.56 ml/min, respectively (Table 4).

**Parameter estimates for  $CL_{int,sec}$ ,  $CL_{int,sec}\{mi\}$ ,  $CL_{int,met}^{D \rightarrow Mi}$  and  $CL_{int,met}^{Mi \rightarrow D}\{mi\}$ .** With assignment of  $CL_{in}$ ,  $CL_{in}\{mi\}$ ,  $CL_{ef}$ , and  $CL_{ef}\{mi\}$ , fitting of the model to the Wistar data yielded 1.90 and 2.54 ml/min, respectively, for  $CL_{int,sec}$  and  $CL_{int,sec}\{mi\}$  and 22.4 and 4.81 ml/min, respectively, for  $CL_{int,met}^{D \rightarrow Mi}$  and  $CL_{int,met}^{Mi \rightarrow D}\{mi\}$ . Since the Sult1e1 expression in TR<sup>-</sup> rat livers was similar to that in Wistar rat livers, a value of 22.4 ml/min was assigned to  $CL_{int,met}^{D \rightarrow Mi}$ , and the corresponding  $CL_{int,met}^{Mi \rightarrow D}\{mi\}$  according to Eq. 3, was calculated to be 31.1 ml/min, for TR<sup>-</sup> group. By contrast, values of 19 and 12.1 ml/min were estimated for  $CL_{int,met}^{Mi \rightarrow D}\{mi\}$  of the Wistar and TR<sup>-</sup> rat livers upon scale-up of the apparent in vitro, microsomal desulfation intrinsic clearance ( $CL_{int,met}^{Mi \rightarrow D}\{mi\}$  in vitro = 0.11 and 0.07  $\mu$ l/s/mg microsomal protein), after multiplication by the scale-up factor (45 mg microsomal protein/g liver tissue) (Houston and Carlile, 1997), yielding an in vitro Wistar/TR<sup>-</sup> desulfation activity ratio of 1.57 (0.11/0.07 or 19/12.1) that differed from the ratio estimated from fitting and the steady-state strategy in perfusion studies (0.155 or 4.81/31.1 using Eq. 3; Table 4). The discrepancy was most likely due to the assumption that  $f_B = f_B\{mi\} = f_L = f_L\{mi\}$  in Equations 1, 2, and 3, and that values reported in Table 4 for the transporter and metabolic intrinsic clearances were only the “effective” or “apparent” intrinsic clearances that could be modified by the unbound fractions. Values of  $CL_{int,sec}$  and  $CL_{int,sec}\{mi\}$  for the TR<sup>-</sup> rat were optimized by trial and error simulations and found to be 0.02 and 0.008 ml/min, respectively (Table 4). These values were very low and almost zero, as expected for the TR<sup>-</sup> rat.

The optimized parameters summarized in Table 4 were used to simulate E<sub>2</sub>17G and E<sub>2</sub>3S17G data in reservoir perfusate, liver, and bile based on the PBPK model for the Wistar and TR<sup>-</sup> livers with the program Micromath Scientist (St. Louis, MO). As shown in Figs. 3C and 3D (blood and bile), the experimental data for the TR<sup>-</sup> group was well predicted by the simulations

based on the rationally chosen set of model parameters (Table 4). The parameter  $ef_m''$ , effective coefficient for metabolite formation that denotes the effect of futile cycling on the disposition of the precursor, decreased from 0.346 in the Wistar liver to almost zero in the TR<sup>-</sup> liver (Table 4), suggesting that alteration in secretory intrinsic clearance of the metabolite would greatly affect the disposition of the precursor in the presence of the futile cycling. The value of  $ef_m'$ , the effective recycling coefficient, was reduced from 0.078 in the Wistar liver to 0.0009 in the TR<sup>-</sup> rat liver (Table 4), suggesting that again, reduction of the secretory intrinsic clearance of drug would affect the disposition of the metabolite in the presence of futile cycling. The low value of  $ef_m'$  was due to the high value of  $CL_{int,met}^{D \rightarrow Mi}$  (22.4 ml/min) in relation to  $CL_{int,met}^{other}$  (= 0) and  $CL_{int,sec}$  in both Wistar (1.9 ml/min) and TR<sup>-</sup> (0.02 ml/min) rats. The reduction in  $ef_m''$  and  $ef_m'$  in the TR<sup>-</sup> livers to those in the Wistar livers in futile cycling was attributed to reduced secretion upon reduction of Mrp2 activity.

### Simulations based on solve solutions for AUCs and clearances

As shown in Fig. 4,  $AUC_R$  (Fig. 4A) and  $AUC_L$  (Fig. 4B) for E<sub>2</sub>17G and E<sub>2</sub>3S17G were both low due to rapid excretion into bile. The  $AUC_R$ 's and  $AUC_L$ 's for both the precursor and formed metabolite increased gradually upon the loss of Mrp2 activity for E<sub>2</sub>17G and E<sub>2</sub>3S17G. When the majority of Mrp2 activity was blunted (>80%), values of the  $AUC_R$ 's and  $AUC_L$ 's for both E<sub>2</sub>17G and E<sub>2</sub>3S17G were elevated precipitously towards infinity (Fig. 4A and 4B). Correspondingly, all the liver clearances were decreased upon the reduction of Mrp2 activity and the values approached zero (Fig. 4C). These scenarios were expected to occur when a potent Mrp2 inhibitor was present, or when Mrp2 was genetically knocked-out as for the mutant (TR<sup>-</sup>) rat. The simulation predicted observations in this communication: when Mrp2 activity was almost abolished in TR<sup>-</sup> rat livers, steady-state would be reached for E<sub>2</sub>17G and E<sub>2</sub>3S17G, the precursor-

metabolite pair that undergoes futile cycling, with the  $AUC_R$  and  $AUC_R\{mi,P\}$  approaching infinity (Fig. 4A) and clearances nearing towards zero (Fig. 4C).

### Other Simulations for AUCs and clearances

Two hypothetical simulations were conducted to mimic more general scenarios in which the parent drug and the metabolite do not share the same canalicular transporter. Again, the parameter values for the Wistar rat liver were used for the simulation (see Table 4). As shown in Fig. 5 (Case 1),  $AUC_R$  and  $AUC_R\{mi,P\}$  (Fig. 5A) and  $AUC_L$  and  $AUC_L\{mi,P\}$  (Fig. 5B) for the precursor and metabolite were increased when the secretory transporter activity of the metabolite but not the parent drug was reduced. The extent of change was not as dramatic as when both the precursor and metabolite secretory transporter activities were blunted (Figs. 4A and B). With the loss of biliary secretion of the metabolite, the net metabolic clearance decreased due to increased futile cycling; this led to an apparent increase in the excretory clearance and decrease in the net metabolic clearance for the precursor. The total liver clearance was decreased.

In the second simulation (Case 2), where there was loss of secretory transporter activity for the parent drug and not the metabolite, the  $AUC_R$  was increased only very slightly but the  $AUC_L$  was evidently elevated, as shown in Fig. 6A and 6B. The excretory clearance of the precursor was decreased and the metabolic clearance was increased, as expected of competing pathways (Liu and Pang, 2005); the total liver clearance was decreased (Fig. 6C). These changes were not as dramatic as Case 1, since the inhibited pathway (excretion of precursor) was not a major elimination pathway relative to that for sulfation, and the  $CL_{int,sec}$  of the precursor was less than 1/10 that of  $CL_{int,met}^{D \rightarrow Mi}$ .

## DISCUSSION

The futile cycling between a precursor-metabolite is a complex relationship. Previous examples of interconversion had revealed parallel decay half-lives of drug and metabolite, and AUC relationships that allowed interconversion metabolic intrinsic clearances to be estimated (Wagner et al., 1981; Ebling and Jusko, 1986; Ferry and Wagner 1986; Aarons, 1987; Cheng and Jusko, 1990a, 1990b, 1990c, 1991, 1993a and 1993b). These solutions mainly pertain to flow-limited substrates and lack consideration of transporters. Later modeling of 4-methylumbelliferone and its sulfate (Ratna et al., 1993; Chiba et al., 1998) and estrone and estrone sulfate, other compounds that undergo futile cycling, has evoked consideration of sinusoidal and canalicular transporters, and revealed the influence of lack of substrate equilibration on futile cycling kinetics (Tan et al., 2001).

With intentions of defining of the role of membrane transporters and enzymes, we had previously employed the PBPK model that describes transporter- and enzyme-mediated processes, such as basolateral influx, efflux, canalicular secretion, and metabolism, and allows one to appraise the significance of rate-limited pathways and transporter-enzyme interplay (de Lannoy et al., 1993; Liu and Pang, 2005; Shitara et al., 2006; Sun et al., 2006; Sun and Pang, 2010). However, most of the focus was on precursor-metabolite pairs that undergo irreversible metabolism, and  $AUC_R\{mi,P\}$  of the formed metabolite was found to be modulated by eliminatory parameters of the precursor and not vice versa (de Lannoy et al., 1993; Pang et al., 2008) (Table 1 and 2 when  $CL_{int,met}^{Mi \rightarrow D}\{mi\} = 0$ ). Upon incorporation of interconversion between the precursor and metabolite and alternate metabolic pathways in present PBPK model, we provided analytical solutions and showed that, in the presence of futile cycling, the eliminatory parameters of the metabolite would affect the disposition of the precursor (Table 2). We unveiled two coefficients

that can modulate the  $AUC_R$  and  $AUC_R\{mi,P\}$  in futile cycling. These are the effective metabolism coefficient,  $ef_m''$ , and the effective recycling coefficient,  $ef_m'$ , which serve as modulators of  $CL_{int,met}^{D \rightarrow Mi}$  and  $CL_{int,met}^{Mi \rightarrow D}\{mi\}$ , respectively. When futile cycling is absent ( $CL_{int,met}^{Mi \rightarrow D}\{mi\} = 0$ ),  $ef_m''$  equals unity. With futile cycling, the  $ef_m''$  value is less than unity, and a lower  $ef_m''$  renders a more pronounced effect on precursor disposition. The value of  $ef_m'$  or  $\frac{CL_{int,sec} + CL_{int,met}^{other}}{CL_{int,sec} + CL_{int,met}^{D \rightarrow Mi} + CL_{int,met}^{other}}$  is not affected by the presence or absence of futile cycling. In the presence of futile cycling,  $ef_m'$  modifies  $CL_{int,met}^{Mi \rightarrow D}\{mi\}$  and thus affects the disposition of the metabolite: a lower  $AUC\{mi,P\}$  arises from a higher  $ef_m'$ .

Experimentally, we illustrated the interplay between Phase II excretion and sulfation and desulfation enzymes with data from Wistar rats as controls and TR<sup>-</sup> rats as the Mrp2-deficient livers in liver perfusion studies. First we identified changes in hepatic Mrp2 and Mrp3 as well as microsomal, desulfation activities, but not in the protein expression of other transporters and sulfotransferases between the two rat strains (Fig. 2). The compensatory increase of Mrp3 protein in TR<sup>-</sup> vs. Wistar rats (Fig. 2) is consistent with other reports (Johnson et al., 2006), though the change was slightly lower. Changes of similar orders of magnitude were also observed for TR<sup>-</sup> rats originating from the same laboratory, with Mrp3 ratios for TR<sup>-</sup> vs. Wistar varying from 6 to 12x (Johnson et al., 2006 and Zamek-Gliszczynski et al., 2006). Our slightly lower ratio of 4.2 obtained could conceivably be due to differences in sample handling and preparation or the variability inherent of the semi-quantitative nature of Western blotting. Dramatic changes in perfusate decay and biliary excretion profiles of Wistar vs. TR<sup>-</sup> perfusion studies were observed (Fig. 3). Expectedly, biliary excretion of E<sub>2</sub>17G and E<sub>2</sub>3S17G was almost abolished in TR<sup>-</sup> rats (Figs. 3B and D, and Table 3), confirming that Mrp2 is the predominant transporter for biliary

excretion of both species (Morikawa et al., 2000). In the TR<sup>-</sup> liver, absence of Mrp2 for the excretion of E<sub>2</sub>17G and E<sub>2</sub>3S17G that undergo futile cycling, together with the compensatory increase of Mrp3, diverted both E<sub>2</sub>17G and E<sub>2</sub>3S17G into reservoir perfusate that reached near plateau levels (Fig. 3C). Due to absence of Mrp2 and abolition of the excretion pathway, most of the radioactivities associated with [<sup>3</sup>H]E<sub>2</sub>17G and [<sup>3</sup>H]E<sub>2</sub>3S17G were trapped in the TR<sup>-</sup> rat liver (Table 3).

Modeling of the data proved to be challenging. Fitting of the model to the Wistar data was not all that successful unless the basolateral influx and efflux clearances were assigned due to the complexity of futile cycling. As shown by previous perfusion studies (Sun et al., 2006), the uptake mechanism of E<sub>2</sub>17G was rapid; and the same was assumed for E<sub>2</sub>3S17G since it was documented that 80% radioactivity of [<sup>3</sup>H]E<sub>2</sub>3S17G appeared rapidly in bile within 15 min after intravenous dosing (Slikker et al., 1983) and simulations based on low CL<sub>in</sub>{mi} for E<sub>2</sub>3S17G resulted in poor predictions. Moreover, no inhibition was found for E<sub>2</sub>3S17G on the uptake of E<sub>2</sub>17G in basolateral membrane vesicles prepared from male Sprague-Dawley rat livers (Vore and Hoffman, 1994).

The relationships extracted from the steady-state (Eqs. 1 to 3), together with the comparison of immunoblots, proved to be a useful strategy to provide parameters for the simulation of E<sub>2</sub>17G and E<sub>2</sub>3S17G profiles in perfusate, liver, and bile to match the experimental data (Fig. 3) for the extremely complex PBPK model (Fig. 1). The approach, though not ideal, offers an alternative to data fitting which failed to converge or resulted in parameters associated with high standard deviations. The estimated parameters, when compared to those of Sun et al. (2006), revealed strain differences. Higher sulfation extents in Wistar vs. Wag/Rij rat livers at 2 h (77±6% vs. 37 ± 5% dose (Sun et al., 2006); Table 4) were noted. This may be explained by enhanced sulfation coupled with faster excretion of E<sub>2</sub>3S17G by Mrp2 in the Wistar vs. Wag/Rij

rat. The  $CL_{ef}$ 's for Wistar and TR<sup>-</sup> rat livers estimated were found to be of low values, and that for the Wag/Rij liver was almost zero (Sun et al., 2006). These values were again very low compared to the extremely rapid influx ( $CL_{in}$ 's) assigned for E<sub>2</sub>17G (Table 4). Data from the TR<sup>-</sup> rat model, however, support the notion that  $CL_{ef\{mi\}}$  was appreciable due to the elevated Mrp3, since accumulation of E<sub>2</sub>3S17G in perfusate was observed. A discrepancy existed on the desulfation intrinsic clearances, estimated as 1.57 in vitro and 0.155 ex vivo (Table 4). This may be explained to be due to the arbitrary assumption that expected of the unbound fractions of E<sub>2</sub>17G and E<sub>2</sub>3S17G in liver tissue to equal those in perfusate and sinusoidal blood. The actual binding could also differ between the Wistar and TR<sup>-</sup> strains, affecting the apparent estimates of the secretory, metabolic, and efflux clearances. The initial decay of E<sub>2</sub>17G in the perfusate was slightly underestimated (Fig. 3A). This may be due to the assumption in PBPK modeling that the tubing volume (~20 ml or ~10% reservoir volume) of the perfusion apparatus was negligible, with the drug concentration in the tubing being identical to that in the reservoir. However for a highly cleared compound such as E<sub>2</sub>17G, the drug in the tubing may decay much faster than that in the reservoir due to the lack of mixing with the returning perfusate. Hence, the PBPK model that does not consider the tubing as a separate compartment may underestimate the decay.

The analytical solutions, the experimental data and model simulations do support the view that a reduction in the excretion of E<sub>2</sub>17G and E<sub>2</sub>3S17G by Mrp2 affects futile cycling kinetics and reduces the net metabolism of E<sub>2</sub>17G. Ordinarily, metabolite parameters would not impact parent drug processing (Pang et al., 2008). However, metabolite and drug parameters do impact the net metabolism, via the coefficient,  $ef_m$  when futile cycling exists (Table 2). Moreover, with a reduction in excretory activities towards the metabolite and drug, both  $ef_m$  and  $ef_m'$  would be reduced (cf. Wistar and TR<sup>-</sup> rats; see Table 5). Under these conditions, both drug and metabolite

AUC's would increase. In fact, a pseudo steady state emerges with futile cycling. The shutdown of biliary excretion of both E<sub>2</sub>17G and E<sub>2</sub>3S17G in the absence of Mrp2 reduced both excretory clearance to almost zero and the total liver clearance (~0); the net formation of E<sub>2</sub>3S17G from E<sub>2</sub>17G was reduced. This first demonstration allows a deeper understanding of the transporter-enzyme interplay of precursor-product relationships, and how metabolite excretion exerts an impact on the net metabolism of the parent drug. The interplay between transporter and enzyme in drug and metabolite processing that was described as a see-saw phenomenon for irreversible metabolic events (Liu and Pang, 2005) has now been extended for futile cycling.

## References

- Aarons L (1987) Mean residence time for drugs subject to reversible metabolism. *J Pharm Pharmacol* **39**:565-567.
- Baillie TA, Halpin RA, Matuszewski BK, Geer LA, Chavez-Eng CM, Dean D, Braun M, Doss G, Jones A, Marks T, Melillo D, and Vyas KP (2001) Mechanistic studies on the reversible metabolism of rofecoxib to 5-hydroxyrofecoxib in the rat: evidence for transient ring opening of a substituted 2-furanone derivative using stable isotope-labeling techniques. *Drug Metab Dispos* **29**:1614-1628.
- Cattori V, van Montfoort JE, Stieger B, Landmann L, Meijer DK, Winterhalter KH, Meier PJ, and Hagenbuch B (2001) Localization of organic anion transporting polypeptide 4 (Oatp4) in rat liver and comparison of its substrate specificity with Oatp1, Oatp2 and Oatp3. *Pflueg Arch Eur J Physiol* **443**: 188–195.
- Cheng H and Jusko WJ (1990a) Constant-rate intravenous infusion methods for estimating steady-state volumes of distribution and mean residence times in the body for drugs undergoing reversible metabolism. *Pharm Res* **7**:628-632.
- Cheng H and Jusko WJ (1993a) Mean residence time of oral drugs undergoing first-pass and linear reversible metabolism. *Pharm Res* **10**:8-13.
- Cheng H and Jusko WJ (1993b) Pharmacokinetics of reversible metabolic systems. *Biopharm Drug Dispos* **14**:721-766.
- Cheng HY and Jusko WJ (1990b) Mean interconversion times and distribution rate parameters for drugs undergoing reversible metabolism. *Pharm Res* **7**:1003-1010.
- Cheng HY and Jusko WJ (1990c) Mean residence times of multicompartmental drugs undergoing reversible metabolism. *Pharm Res* **7**:103-107.
- Cheng HY and Jusko WJ (1991) Mean residence times and distribution volumes for drugs undergoing linear reversible metabolism and tissue distribution and linear or nonlinear elimination from the central compartments. *Pharm Res* **8**:508-511.
- Chiba M, Schwab AJ, Goresky CA, and Pang KS (1998) Carrier-mediated entry of 4-methylumbelliferyl sulfate: characterization by the multiple-indicator dilution technique in perfused rat liver. *Hepatology* **27**:134-146.
- de Lannoy IA, Barker F 3<sup>rd</sup>, and Pang KS (1993) Formed and preformed metabolite excretion clearances in liver, a metabolite formation organ: studies on enalapril and enalaprilat in the single-pass and recirculating perfused rat liver. *J Pharmacokinet Biopharm* **21**:395-422.
- Ebling WF and Jusko WJ (1986) The determination of essential clearance, volume, and residence time parameters of recirculating metabolic systems: the reversible metabolism of methylprednisolone and methylprednisone in rabbits. *J Pharmacokinet Biopharm* **14**:557-599.

Ferry JJ, Jr. and Wagner JG (1986) The non-linear pharmacokinetics of prednisone and prednisolone. I. Theoretical. *Biopharm Drug Dispos* **7**:91-101.

Grubb NG, Rudy DW, Brater DC, and Hall SD (1999) Stereoselective pharmacokinetics of ketoprofen and ketoprofen glucuronide in end-stage renal disease: evidence for a 'futile cycle' of elimination. *Br J Clin Pharmacol* **48**:494-500.

Hansel SB and Morris ME (1996) Hepatic conjugation/deconjugation cycling pathways. Computer simulations examining the effect of Michaelis-Menten parameters, enzyme distribution patterns, and a diffusional barrier on metabolite disposition. *J Pharmacokinet Biopharm* **24**:219-243.

Houston JB and Carlile DJ (1997) Prediction of hepatic clearance from microsomes, hepatocytes, and liver slices. *Drug Metab Rev* **29**:891-922.

Ito K, Suzuki H, Hirohashi T, Kume K, Shimizu T, and Sugiyama Y (1997) Molecular cloning of canalicular multispecific organic anion transporter defective in EHBR. *Am J Physiol* **272**:G16-G22.

Jansen PL, Peters WH, and Lamers WH (1985) Hereditary chronic conjugated hyperbilirubinemia in mutant rats caused by defective hepatic anion transport. *Hepatology* **5**:573-579.

Johnson BM, Zhang P, Schuetz JD, and Brouwer KL (2006) Characterization of transport protein expression in multidrug resistance-associated protein (Mrp) 2-deficient rats. *Drug Metab Dispos* **34**:556-562.

Kauffman FC, Sharp S, Allan BB, Burchell A, and Coughtrie MW (1998) Microsomal steroid sulfatase: interactions with cytosolic steroid sulfotransferases. *Chem Biol Interact* **109**:169-82.

Liu L and Pang KS (2005) The roles of transporters and enzymes in hepatic drug processing. *Drug Metab Dispos* **33**:1-9.

Lowry OH, Rosebrough NJ, Farr AL, and Randall RJ (1951) Protein measurement with the Folin phenol reagent. *J Biol Chem* **193**:265-275.

Meffin PJ, Zilm DM, and Veenendaal JR (1983) Reduced clofibrilic acid clearance in renal dysfunction is due to a futile cycle. *J Pharmacol Exp Ther* **227**:732-738.

Morikawa A, Goto Y, Suzuki H, Hirohashi T, and Sugiyama Y (2000) Biliary excretion of 17 $\beta$ -estradiol 17 $\beta$ -D-glucuronide is predominantly mediated by cMOAT/MRP2. *Pharm Res* **17**:546-552.

Müller M, Roelofsen H, and Jansen PL (1996) Secretion of organic anions by hepatocytes: involvement of homologues of the multidrug resistance protein. *Semin Liver Dis* **16**:211-220.

Pang KS, Lee WF, Cherry WF, Yuen V, Accaputo J, Fayz S, Schwab AJ, and Goresky CA (1988) Effects of perfusate flow rate on measured blood volume, disse space, intracellular water space, and drug extraction in the perfused rat liver preparation: characterization by the multiple indicator dilution technique. *J Pharmacokinet Biopharm* **16**:595-632.

- Pang KS, Morris ME, and Sun H (2008) Formed and preformed metabolites: facts and comparisons. *J Pharm Pharmacol* **60**:1247-1275.
- Ratna S, Chiba M, Bandyopadhyay L, and Pang KS (1993) Futile cycling between 4-methylumbelliferone and its conjugates in perfused rat liver. *Hepatology* **17**:838-853.
- Shitara Y, Horie T, and Sugiyama Y (2006) Transporters as a determinant of drug clearance and tissue distribution. *Eur J Pharm Sci* **27**:425-446.
- Sirianni GL and Pang KS (1997) Organ clearance concepts: new perspectives on old principles. *J Pharmacokinet Biopharm* **25**:449-70.
- Slikker W, Jr., Vore M, Bailey JR, Meyers M, and Montgomery C (1983) Hepatotoxic effects of estradiol-17 beta-D-glucuronide in the rat and monkey. *J Pharmacol Exp Ther* **225**:138-143.
- Sun H and Pang KS (2010) Physiological modeling to understand the impact of enzymes and transporters on drug and metabolite data and bioavailability estimates. *Pharm Res* in press.
- Sun H, Liu L, and Pang KS (2006) Increased estrogen sulfation of estradiol 17 $\beta$  D-glucuronide in metastatic tumor rat livers. *J Pharmacol Exp Ther* **319**:818-831.
- Tan E, Lu T, and Pang KS (2001) Futile cycling of estrone sulfate and estrone in the recirculating perfused rat liver preparation. *J Pharmacol Exp Ther* **297**:423-436.
- Vore M and Hoffman T (1994) Carrier-mediated electrogenic transport of estradiol-17 beta-glucuronide in rat liver BMV. *Am J Physiol* **267**:G546-G551.
- Wagner JG, DiSanto AR, Gillespie WR, and Albert KS (1981) Reversible metabolism and pharmacokinetics: application to prednisone-prednisolone. *Res Commun Chem Pathol Pharmacol* **32**:387-405.
- Xiong H, Turner KC, Ward ES, Jansen PL, and Brouwer KL (2000) Altered hepatobiliary disposition of acetaminophen glucuronide in isolated perfused livers from multidrug resistance-associated protein 2-deficient TR(-) rats. *J Pharmacol Exp Ther* **295**:512-8.
- Xu X, Selick P, and Pang KS (1993) Nonlinear protein binding and enzyme heterogeneity: effects on hepatic drug removal. *J Pharmacokinet Biopharm* **21**:43-74.
- Zamek-Gliszczynski MJ, Hoffmaster KA, Humphreys JE, Tian X, Nezasa K, and Brouwer KL (2006) Differential involvement of Mrp2 (Abcc2) and Bcrp (Abcg2) in biliary excretion of 4-methylumbelliferyl glucuronide and sulfate in the rat. *J Pharmacol Exp Ther* **319**:459-467.

## Footnote

<sup>1</sup>Present address: NoAb BioDiscoveries Inc, Mississauga, Ontario, Canada

<sup>2</sup>This work is supported by CIHR Grant #MOP89850; Huadong Sun was a recipient of the UofT Open Fellowship.

## Legends

**Figure 1.** Schematic diagram of the physiological based liver model for the transport and metabolism of E<sub>2</sub>17G and its 3-sulfate metabolite (E<sub>2</sub>3S17G). The model is composed of reservoir, sinusoid, hepatocyte, and canaliculus compartment. E<sub>2</sub>17G and E<sub>2</sub>3S17G in the reservoir perfusate are delivered at a flow rate of  $Q_L$  to the sinusoid. The unbound molecule that rapidly equilibrate with the bound ones to albumin and red blood cells in the sinusoid are taken up into the hepatocyte with  $CL_{in}$  and  $CL_{in}\{mi\}$  for E<sub>2</sub>17G and E<sub>2</sub>3S17G, respectively. In the hepatocyte, E<sub>2</sub>17G is sulfated with  $CL_{int,met}^{D \rightarrow Mi}$  and the resultant metabolite, E<sub>2</sub>3S17G, is desulfated back to E<sub>2</sub>17G with  $CL_{int,met}^{Mi \rightarrow D}\{mi\}$ . Both E<sub>2</sub>17G and E<sub>2</sub>3S17G in the hepatocyte may be returned back to the sinusoid with  $CL_{ef}$  and  $CL_{ef}\{mi\}$ , respectively, or excreted into the bile canaliculus with  $CL_{int,sec}$  and  $CL_{int,sec}\{mi\}$ , respectively. Other metabolic pathways,  $CL_{int,met}^{other}$  for the parent and  $CL_{int,met}^{other}\{mi\}$  for the formed metabolite, though of minor significance, have been included to reflect a general scheme. The bile flow rate is  $Q_{bile}$ .

**Figure 2.** Integrated densitometric analysis of crude membrane (for Oatp1a1, Oatp1a4, Oatp1b2, Mrp2, Mrp3 and Mrp4) and cytosolic (Sult1a1 and Sult1e1) fractions prepared from Wistar (solid bar) and TR<sup>-</sup> (open bar) rat liver. Protein expression of the target protein was presented as the ratio of densitometric measurements of the target protein to that of GAPDH. For each target protein, the expression was normalized to the average value in Wistar rat livers.

**Figure 3.** Time-dependent profile of E<sub>2</sub>17G and E<sub>2</sub>3S17G in the perfusate and liver (A, C) and bile (B, D) of recirculating perfused Wistar (A, B) and those in TR<sup>-</sup> (C,D) rat liver preparations (n = 4 for both groups) based on parameters shown in Table 4 and differential equations in the Appendix. For experimental data, E<sub>2</sub>17G was denoted by ● in perfusate and bile and ○ in liver; E<sub>2</sub>3S17G was denoted by ▲ in perfusate and bile and △ in liver. For prediction, E<sub>2</sub>17G was denoted by —

— in perfusate and bile and —·—· in liver; E<sub>2</sub>3S17G was denoted by ----- in perfusate and bile and —·—· in liver.

**Figure 4.** Simulated profiles for (A) AUC<sub>R</sub> for E<sub>2</sub>17G (—) and AUC<sub>R</sub>{mi,P} for E<sub>2</sub>3S17G (---) in reservoir, (B) AUC<sub>L</sub> for E<sub>2</sub>17G (—) and AUC<sub>L</sub>{mi,P} for E<sub>2</sub>3S17G (-----) in liver, and (C) the resultant metabolic (-----), excretory (—·—·), and total (—) liver clearances of E<sub>2</sub>17G upon reduction/loss of Mrp2 activity.

**Figure 5.** Simulated profiles for (A) AUC<sub>R</sub> for E<sub>2</sub>17G (—) and AUC<sub>R</sub>{mi,P} for E<sub>2</sub>3S17G (---) in reservoir, (B) AUC<sub>L</sub> for E<sub>2</sub>17G (—) and AUC<sub>L</sub>{mi,P} for E<sub>2</sub>3S17G (-----) in liver, and (C) the resultant metabolic (-----), excretory (—·—·), and total (—) liver clearances of E<sub>2</sub>17G upon reduction/loss of Mrp2 activity: This simulation described Mrp2 activity loss of E<sub>2</sub>3S17G only, a hypothetical scenario.

**Figure 6.** Simulated profiles for (A) AUC<sub>R</sub> for E<sub>2</sub>17G (—) and AUC<sub>R</sub>{mi,P} for E<sub>2</sub>3S17G (---) in reservoir, (B) AUC<sub>L</sub> for E<sub>2</sub>17G (—) and AUC<sub>L</sub>{mi,P} for E<sub>2</sub>3S17G (-----) in liver, and (C) the resultant metabolic (-----), excretory (—·—·), and total (—) liver clearances of E<sub>2</sub>17G upon reduction/loss of Mrp2 activity: This simulation described Mrp2 activity loss of E<sub>2</sub>17G only, a hypothetical scenario.

# DMD #29959

**Table 1.** Analytical solutions for the area of the curve from time 0 to infinity for the parent drug ( $AUC_R$  and  $AUC_L$ ) and formed metabolite ( $AUC_R\{mi,P\}$  and  $AUC_L\{mi,P\}$ ) in reservoir and liver tissue and amount of cumulative biliary excretion of the parent drug ( $A_{e,\infty}$ ) and metabolite ( $A_{e,\infty}\{mi,P\}$ ) at time infinity for a drug-metabolite pair in absence ( $CL_{int,met}^{Mi \rightarrow D}\{mi\} = 0$ ) and presence ( $CL_{int,met}^{Mi \rightarrow D}\{mi\} > 0$ ) of futile cycling (see text for definition of terms).

Terms	Solutions
$AUC_R^a$	$\frac{\text{Dose} \left[ Q_L (CL_{ef} + CL_{int,sec} + ef_m'' CL_{int,met}^{D \rightarrow Mi} + CL_{int,met}^{other}) + f_B CL_{in} (CL_{int,sec} + ef_m'' CL_{int,met}^{D \rightarrow Mi} + CL_{int,met}^{other}) \right]}{Q_L f_B CL_{in} (CL_{int,sec} + ef_m'' CL_{int,met}^{D \rightarrow Mi} + CL_{int,met}^{other})}$
$AUC_R\{mi,P\}^b$	$\frac{\text{Dose} CL_{ef}\{mi\} CL_{int,met}^{D \rightarrow Mi}}{f_B\{mi\} CL_{in}\{mi\} (CL_{int,sec} + CL_{int,met}^{D \rightarrow Mi} + CL_{int,met}^{other}) (CL_{int,sec}\{mi\} + ef_m' CL_{int,met}^{Mi \rightarrow D}\{mi\} + CL_{int,met}^{other}\{mi\})}$
$AUC_L$	$\frac{\text{Dose}}{f_L (CL_{int,sec} + CL_{int,met}^{other} + ef_m'' CL_{int,met}^{D \rightarrow Mi})}$
$AUC_L\{mi,P\}$	$\frac{\text{Dose} CL_{int,met}^{D \rightarrow Mi}}{f_L\{mi\} (CL_{int,sec} + CL_{int,met}^{D \rightarrow Mi} + CL_{int,met}^{other}) (CL_{int,sec}\{mi\} + ef_m' CL_{int,met}^{Mi \rightarrow D}\{mi\} + CL_{int,met}^{other}\{mi\})}$
$A_{e,\infty}$	$\frac{\text{Dose} CL_{int,sec}}{(CL_{int,sec} + CL_{int,met}^{other} + ef_m'' CL_{int,met}^{D \rightarrow Mi})}$
$A_{e,\infty}\{mi,P\}$	$\frac{\text{Dose} CL_{int,met}^{D \rightarrow Mi} CL_{int,sec}\{mi\}}{(CL_{int,sec} + CL_{int,met}^{D \rightarrow Mi} + CL_{int,met}^{other}) (CL_{int,sec}\{mi\} + ef_m' CL_{int,met}^{Mi \rightarrow D}\{mi\} + CL_{int,met}^{other}\{mi\})}$

<sup>a</sup>  $ef_m''$ , effective coefficient for metabolite formation,  $ef_m'' = \frac{CL_{int,sec}\{mi\} + CL_{int,met}^{other}\{mi\}}{CL_{int,sec}\{mi\} + CL_{int,met}^{Mi \rightarrow D}\{mi\} + CL_{int,met}^{other}\{mi\}}$ .

In absence of futile cycling,  $CL_{int,met}^{Mi \rightarrow D}\{mi\} = 0$ , rendering  $ef_m'' = 1$ ; in presence of futile cycling,  $CL_{int,met}^{Mi \rightarrow D}\{mi\} > 0$ , rendering  $0 < ef_m'' < 1$ .

<sup>b</sup>  $ef_m'$ , effective recycling coefficient,  $ef_m' = \frac{CL_{int,sec} + CL_{int,met}^{other}}{CL_{int,sec} + CL_{int,met}^{D \rightarrow Mi} + CL_{int,met}^{other}}$ .

Table 2. Analytical solutions for the metabolic ( $CL_{liver,met}$ ), excretory ( $CL_{liver,ex}$ ), and total ( $CL_{liver,tot}$ ) liver clearances in the presence of futile cycling

Clearances <sup>a</sup>	With Barrier	Without Barrier ( $CL_{in} = CL_{ef} \gg CL_{int,sec}$ , $ef_m'' CL_{int,met}^{D \rightarrow Mi}$ , and $CL_{int,met}^{other}$ )
$CL_{liver,ex}$ <sup>b</sup>	$\frac{Q_L f_B CL_{in} CL_{int,sec}}{[Q_L (CL_{ef} + CL_{int,sec} + ef_m'' CL_{int,met}^{D \rightarrow Mi} + CL_{int,met}^{other}) + f_B CL_{in} (CL_{int,sec} + ef_m'' CL_{int,met}^{D \rightarrow Mi} + CL_{int,met}^{other})]}$	$\frac{Q_L f_B CL_{int,sec}}{[Q_L + f_B (CL_{int,sec} + ef_m'' CL_{int,met}^{D \rightarrow Mi} + CL_{int,met}^{other})]}$
$CL_{liver,met}$	$\frac{Q_L f_B CL_{in} (ef_m'' CL_{int,met}^{D \rightarrow Mi} + CL_{int,met}^{other})}{[Q_L (CL_{ef} + CL_{int,sec} + ef_m'' CL_{int,met}^{D \rightarrow Mi} + CL_{int,met}^{other}) + f_B CL_{in} (CL_{int,sec} + ef_m'' CL_{int,met}^{D \rightarrow Mi} + CL_{int,met}^{other})]}$	$\frac{Q_L f_B (ef_m'' CL_{int,met}^{D \rightarrow Mi} + CL_{int,met}^{other})}{[Q_L + f_B (CL_{int,sec} + ef_m'' CL_{int,met}^{D \rightarrow Mi} + CL_{int,met}^{other})]}$
$CL_{liver,tot}$	$\frac{Q_L f_B CL_{in} (CL_{int,sec} + ef_m'' CL_{int,met}^{D \rightarrow Mi} + CL_{int,met}^{other})}{[Q_L (CL_{ef} + CL_{int,sec} + ef_m'' CL_{int,met}^{D \rightarrow Mi} + CL_{int,met}^{other}) + f_B CL_{in} (CL_{int,sec} + ef_m'' CL_{int,met}^{D \rightarrow Mi} + CL_{int,met}^{other})]}$	$\frac{Q_L f_B (CL_{int,sec} + ef_m'' CL_{int,met}^{D \rightarrow Mi} + CL_{int,met}^{other})}{[Q_L + f_B (CL_{int,sec} + ef_m'' CL_{int,met}^{D \rightarrow Mi} + CL_{int,met}^{other})]}$

<sup>a</sup> The solutions for the total hepatic ( $CL_{liver,total}$ ) and the excretory ( $CL_{liver,ex}$ ) clearances were obtained by  $Dose/AUC_R$  and  $A_{e,\infty}/AUC_R$ , respectively. The metabolic clearance was estimated by the difference of  $CL_{liver,total}$  and  $CL_{liver,ex}$ .

<sup>b</sup>  $ef_m''$ , effective coefficient for metabolite formation,  $ef_m'' = \frac{CL_{int,sec} \{mi\} + CL_{int,met}^{other} \{mi\}}{CL_{int,sec} \{mi\} + CL_{int,met}^{Mi \rightarrow D} \{mi\} + CL_{int,met}^{other} \{mi\}}$

DMD #29959

Table 3. Experimentally derived parameters for the *in situ* recirculating perfused Wistar and TR<sup>-</sup> rat liver preparations, with dosing of [<sup>3</sup>H]E<sub>2</sub>17G (~ initial concentration of 100,000 dpm/ml) into the reservoir <sup>a</sup>

Experimental Parameters	Wistar	TR <sup>-</sup>
Rat body weight (g)	329 ± 21	283 ± 11 <sup>c</sup>
Rat liver weight (g)	13.7 ± 2.3	13.7 ± 0.9
Hematocrit (Hct)	0.14 ± 0.01	0.14 ± 0.01
Perfusate flow rate, Q <sub>L</sub> (ml/min)	12	12
Bile flow rate, Q <sub>bile</sub> (μl/min)	6.3 ± 0.7	2.4 ± 0.5 <sup>d</sup>
Perfusate volume recovery at 2 h (%)	91 ± 3	91 ± 2
Dose in perfusate at 2 h (%)	0.6 ± 0.2	17.0 ± 2.0
E <sub>2</sub> 17G in perfusate at 2 h (%)	n.d. <sup>e</sup>	9.0 ± 1.3 <sup>d</sup>
E <sub>2</sub> 3S17G in perfusate at 2 h (%)	n.d. <sup>e</sup>	12.2 ± 1.4
Dose in liver tissue at 2 h (%)	3.9 ± 2.7	66 ± 6 <sup>d</sup>
E <sub>2</sub> 17G in liver tissue at 2 h (%)	1.4 ± 0.7	39 ± 9 <sup>d</sup>
E <sub>2</sub> 3S17G in liver tissue at 2 h (%)	2.5 ± 2.1	28 ± 5 <sup>d</sup>
Dose in bile at 2 h (%)	92 ± 6	1.8 ± 0.4 <sup>d</sup>
E <sub>2</sub> 17G in bile at 2 h (%)	17 ± 4	1.3 ± 0.3 <sup>d</sup>
E <sub>2</sub> 3S17G in bile at 2 h (%)	75 ± 5	0.4 ± 0.1 <sup>d</sup>
Total E <sub>2</sub> 3S17G at 2 h (%) <sup>b</sup>	77 ± 6	40 ± 6 <sup>d</sup>
Dose recovery at 2 h (%)	100 ± 6	90 ± 4
AUC <sub>0-45 min</sub> (min)	1588 ± 195	1455 ± 86
AUC <sub>0-120 min</sub> (min)	n.a. <sup>f</sup>	2161 ± 111
AUC <sub>0-∞</sub> (min)	1697 ± 226	close to ∞ <sup>d</sup>

<sup>a</sup> data were presented as mean ± SD, unless specified; the initial amount of E<sub>2</sub>17G in the reservoir perfusate was set to 100 and unitless

<sup>b</sup> sum of amounts in reservoir, liver, and bile

<sup>c,d</sup> *P* < .01 and *P* < .001, respectively, with the Student's *t*-test (n = 4)

<sup>e</sup> the radioactivity was too low to be detected

<sup>f</sup> not applicable since data were not available beyond 45 min

DMD #29959

Table 4. Assigned and estimated parameters used for simulation of E<sub>2</sub>17G and E<sub>2</sub>3S17G profiles/parameters in the recirculating perfused Wistar and TR<sup>-</sup> rat liver preparations according to the liver PBPK model

Parameters	TR <sup>-</sup> Livers	Wistar Livers
V <sub>R</sub> , volume of reservoir (ml)	180 <sup>a</sup>	182 <sup>a</sup>
V <sub>LB</sub> , volume of sinusoid (ml)	1.82 <sup>b</sup>	1.81 <sup>b</sup>
V <sub>L</sub> , volume of liver tissue (ml)	9.11 <sup>b</sup>	9.07 <sup>b</sup>
V <sub>bile</sub> , volume of canaliculi and bile cannula (ml)	0.108 <sup>c</sup>	0.108 <sup>c</sup>
Q <sub>bile</sub> , bile flow rate (μl/min)	2.4 <sup>d</sup>	6.3 <sup>d</sup>
f <sub>B</sub> , f <sub>L</sub> , f <sub>B</sub> {mi}, f <sub>L</sub> {mi}, unbound fractions for E <sub>2</sub> 17G in blood and liver, E <sub>2</sub> 3S17G in perfusate and liver, respectively	0.23 <sup>d</sup>	0.22 <sup>d</sup>
CL <sub>in</sub> , influx clearance for E <sub>2</sub> 17G (ml/min)	546 <sup>e</sup>	546 <sup>e</sup>
CL <sub>ef</sub> , efflux clearance for E <sub>2</sub> 17G (ml/min)	5.75 <sup>f</sup>	1.35 <sup>g</sup>
CL <sub>in</sub> {mi}, influx clearance for E <sub>2</sub> 3S17G (ml/min)	546 <sup>h</sup>	546 <sup>h</sup>
CL <sub>ef</sub> {mi}, efflux clearance for E <sub>2</sub> 3S17G (ml/min)	10.9 <sup>i</sup>	2.56 <sup>g</sup>
CL <sub>int,met</sub> <sup>D→Mi</sup> , sulfation intrinsic clearance (ml/min)	22.4 <sup>j</sup>	22.4 <sup>k</sup>
CL <sub>int,met</sub> <sup>Mi→D</sup> {mi}, desulfation intrinsic clearance (ml/min)	31.1 <sup>l</sup>	4.81 <sup>k</sup>
CL <sub>int,sec</sub> , secretory intrinsic clearance for E <sub>2</sub> 17G (ml/min)	0.02 <sup>m</sup>	1.90 <sup>k</sup>
CL <sub>int,sec</sub> {mi}, E <sub>2</sub> 3S17G secretory intrinsic clearance (ml/min)	0.008 <sup>m</sup>	2.54 <sup>k</sup>
ef <sub>m</sub> '', effective coefficient for metabolite formation	0.00026	0.346
ef <sub>m</sub> ', effective recycling coefficient	0.00089	0.078

<sup>a</sup> averaged value from t=0 (200 ml) to time=2 h

<sup>b</sup> from MID studies (Pang et al., 1988).

<sup>c</sup> sum of bile volume of canaliculi (0.004 ml/g liver) and bile cannula volume (20 cm of polypropylene tubing with i.d. of 0.58 mm)

<sup>d</sup> observations; for unbound fractions, f<sub>B</sub> is the determined value (Sun et al., 2006) and f<sub>L</sub>, f<sub>B</sub>{mi}, and f<sub>L</sub>{mi} were set to equal f<sub>B</sub> for simplicity

<sup>e</sup> assigned, same as Wag/Rij rat liver from Sun et al. (2006), and according to Oatp's protein expression (Fig. 2).

<sup>f</sup> according to Eq. 1

<sup>g</sup> according to ratio of relative Mrp3 protein expression in Fig. 2 (TR<sup>-</sup>/Wistar = 4.2)

<sup>h</sup> based on the assumption that CL<sub>in</sub>{mi} = CL<sub>in</sub>

<sup>i</sup> according to Eq. 2

<sup>j</sup> based on similar protein expressions of Sult's for TR<sup>-</sup> and Wistar rat livers in Fig. 2

<sup>k</sup> estimate for Wistar rat derived from preliminary data fitting, with fixed basolateral influx and efflux parameters

<sup>l</sup> according to Eq. 3

<sup>m</sup> optimized by trial and error

Figure 1

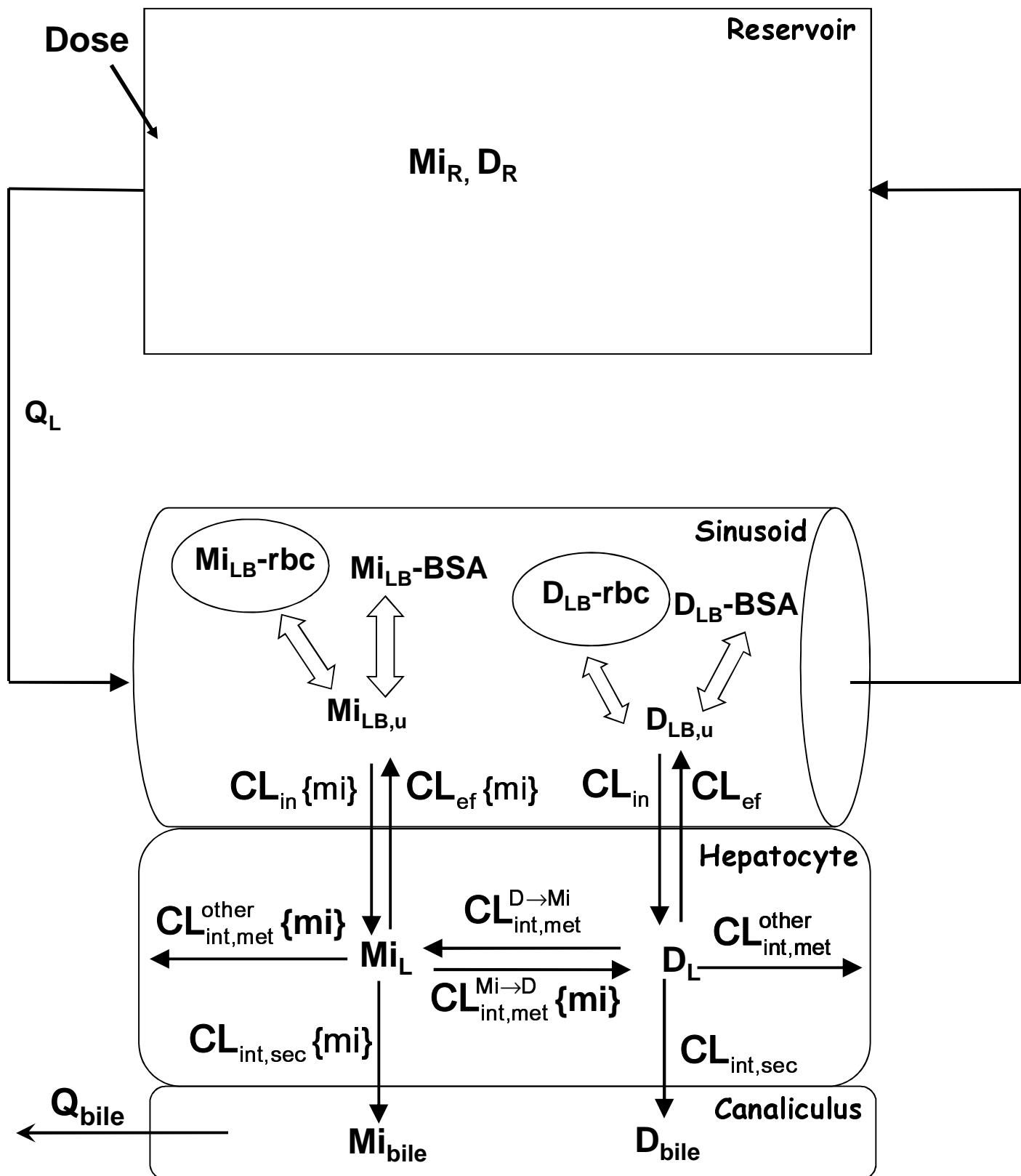


Figure 2

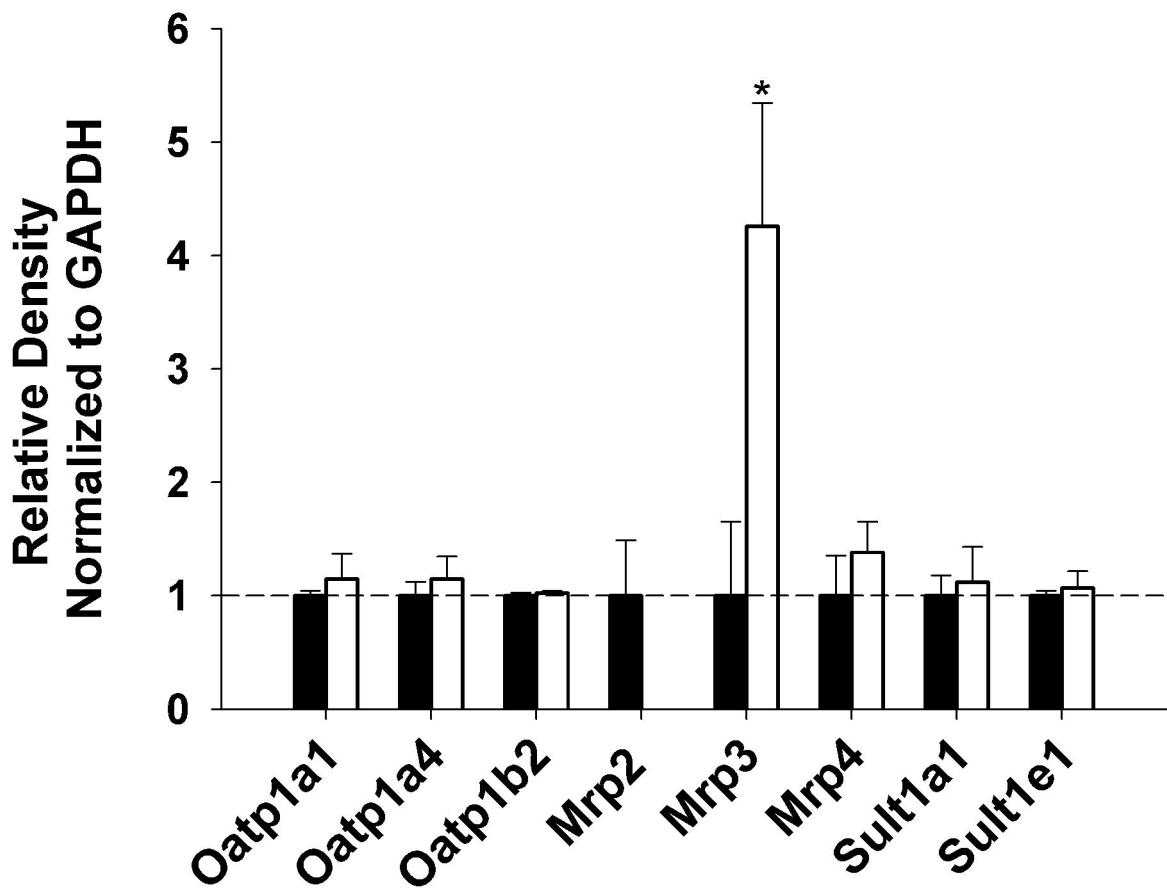


Figure 3

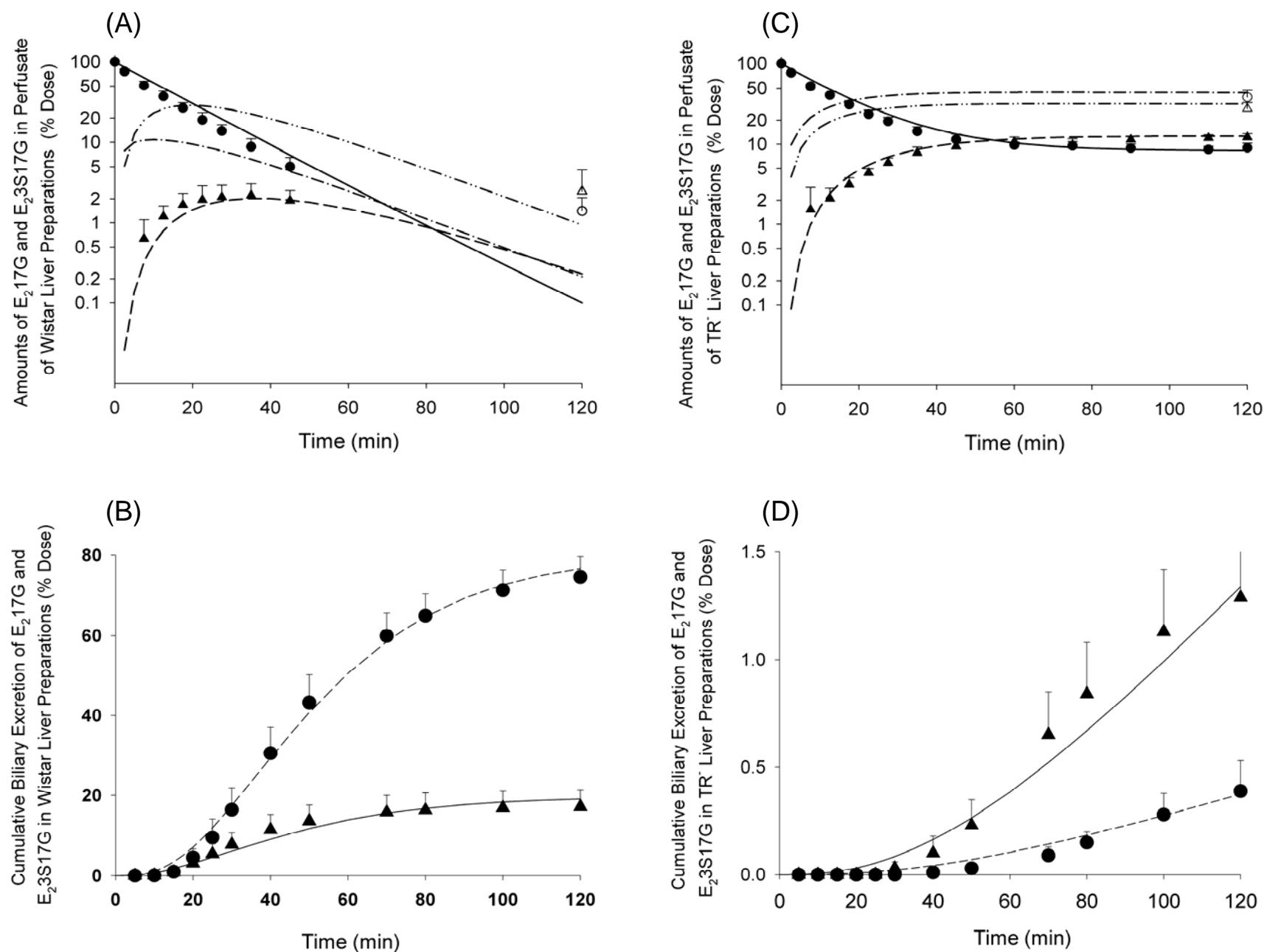


Figure 4

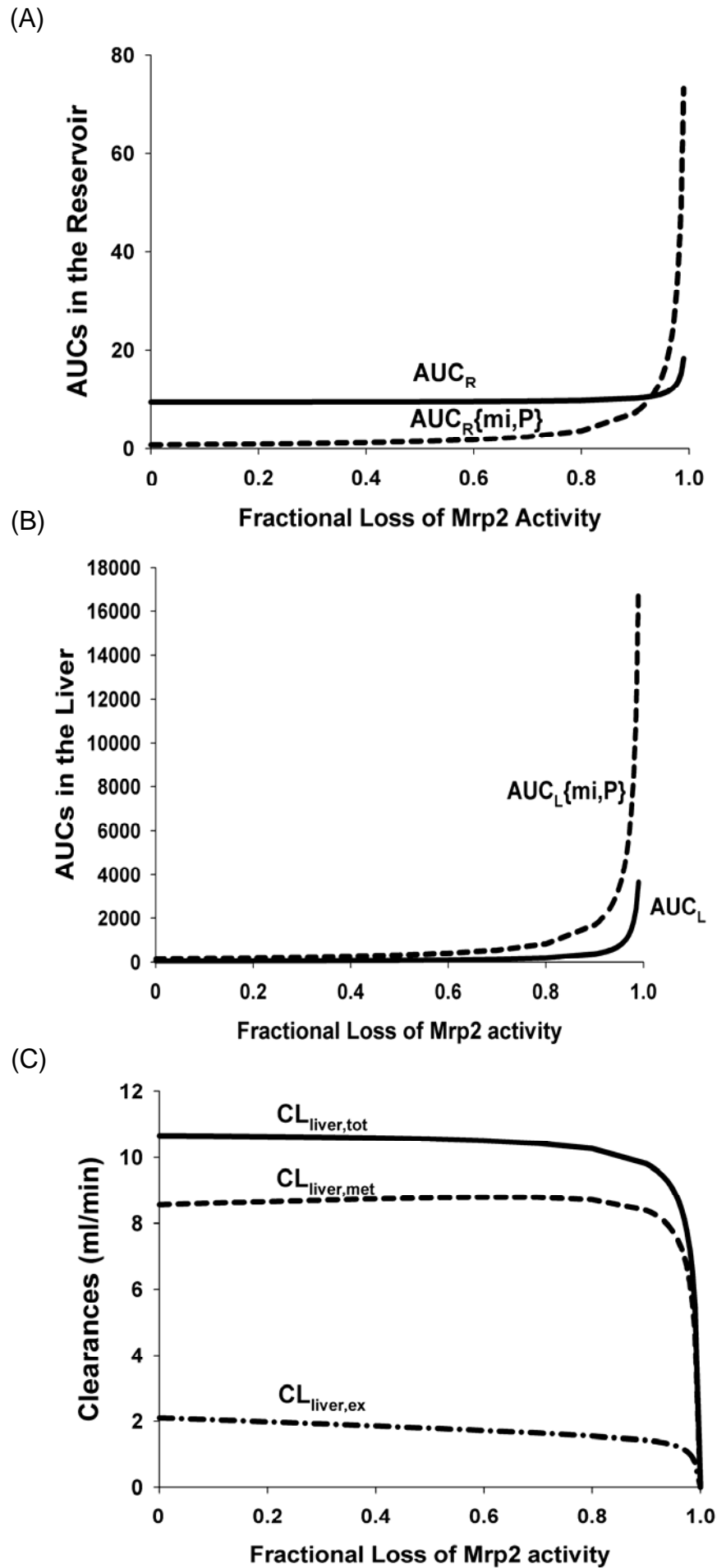


Figure 5

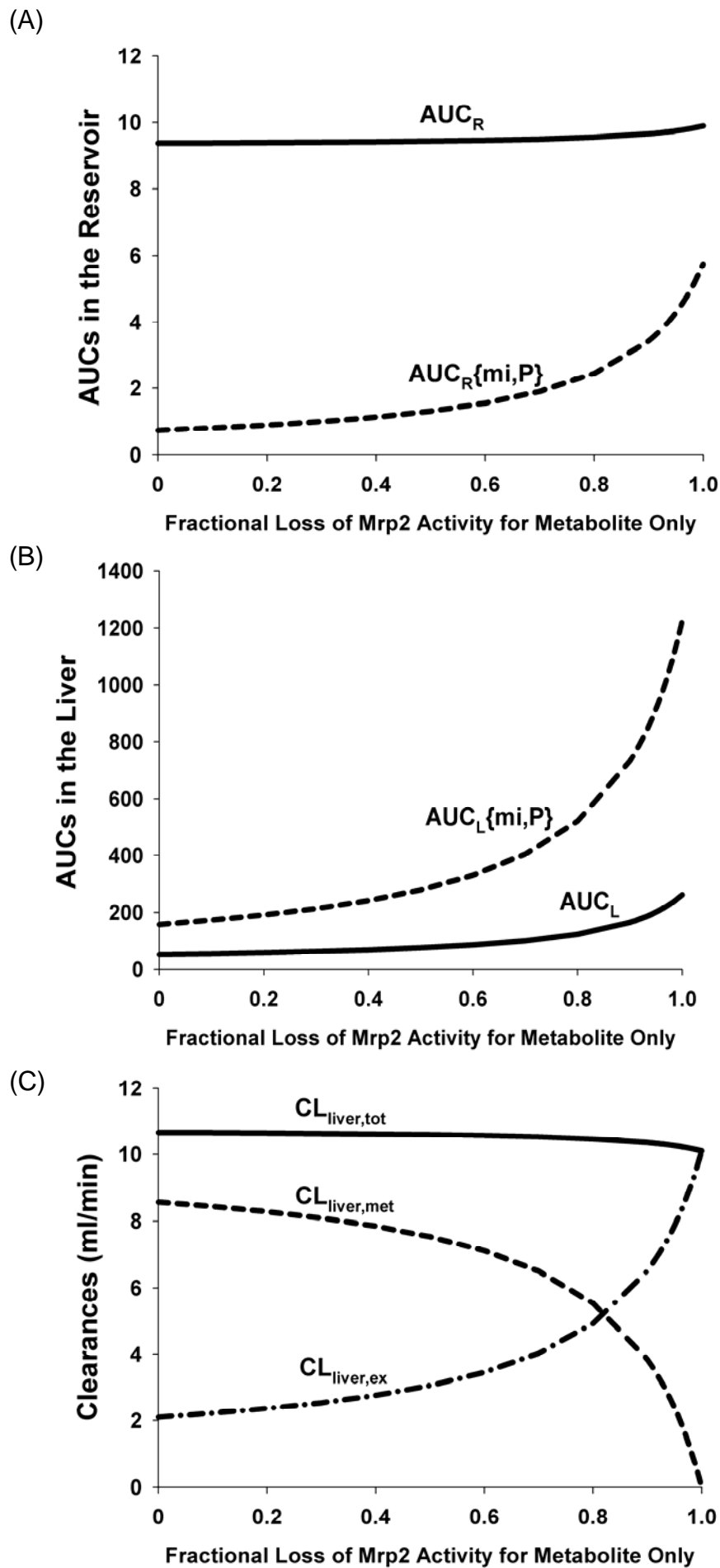
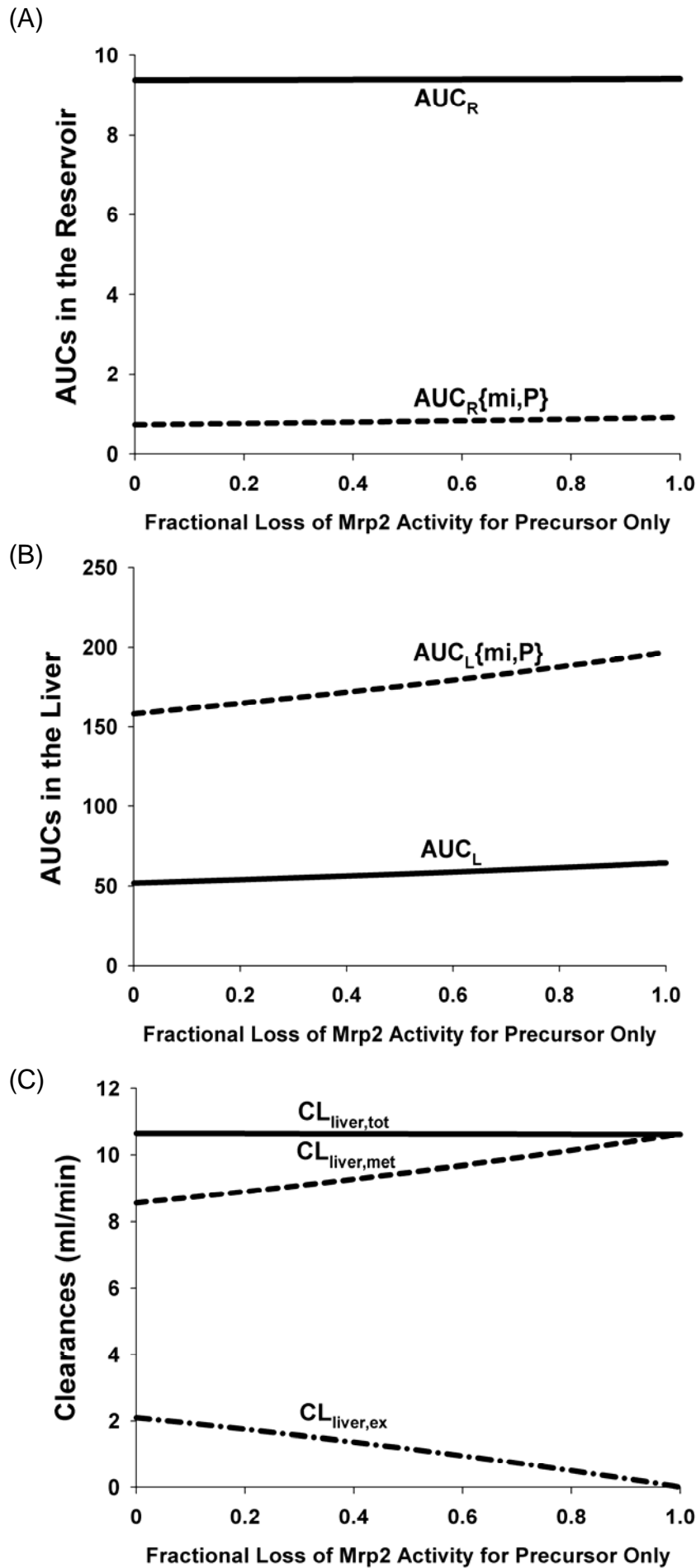


Figure 6



## Appendix

### Mass balance equations for a PBPK model (Fig. 1)

In the following equations, D and Mi denote concentrations of the parent drug (representing E<sub>2</sub>17G) and its formed metabolite (representing E<sub>2</sub>3S17G), respectively. Q<sub>L</sub>, V, and f denote the blood flow rate, the volume in each compartment, and unbound fraction, respectively. The subscripts, R, LB, L, and bile denote reservoir blood, liver blood/sinusoids, liver tissue, and canalicular bile, respectively. Other parameters (intrinsic clearances) have been defined in the Materials and Methods section.

For rates of change of E<sub>2</sub>17G and E<sub>2</sub>3S17G in reservoir blood,

$$V_R \frac{dD_R}{dt} = Q_L (D_{LB} - D_R) \quad (A1)$$

$$V_R \frac{dMi_R}{dt} = Q_L (Mi_{LB} - Mi_R) \quad (A2)$$

For rates of change of E<sub>2</sub>17G and E<sub>2</sub>3S17G in liver blood or the sinusoid,

$$V_{LB} \frac{dD_{LB}}{dt} = Q_L (D_R - D_{LB}) + f_L CL_{ef} D_L - f_{LB} CL_{in} D_{LB} \quad (A3)$$

where  $f_{LB} = f_B = \frac{f_p}{(1-Hct) + D_{RBC}/D_p \times Hct}$ , Hct is the hemotocrit; f<sub>p</sub> is the unbound fraction of the parent

drug in plasma. D<sub>RBC</sub>/D<sub>p</sub> is the drug concentration ratio between red blood cells (RBC) and plasma (p).

$$V_{LB} \frac{dMi_{LB}}{dt} = Q_L (Mi_R - Mi_{LB}) + f_L \{mi\} CL_{ef} \{mi\} Mi_L - f_{LB} \{mi\} CL_{in} \{mi\} Mi_{LB} \quad (A4)$$

For rates of change of E<sub>2</sub>17G and E<sub>2</sub>3S17G in liver tissue,

$$V_L \frac{dD_L}{dt} = f_B D_{LB} CL_{in} + f_L \{mi\} Mi_L CL_{int,met}^{Mi \rightarrow D} \{mi\} - f_L D_L (CL_{ef} + CL_{int,met}^{D \rightarrow Mi} + CL_{int,met}^{other} + CL_{int,sec}) \quad (A5)$$

# DMD #29959

$$V_L \frac{dMi_L}{dt} = f_B \{mi\} CL_{in} \{mi\} Mi_{LB} + f_L CL_{int,met}^{D \rightarrow Mi} D_L - f_L \{mi\} (CL_{ef} \{mi\} + CL_{int,met}^{Mi \rightarrow D} \{mi\} + CL_{int,met}^{other} \{mi\} + CL_{int,sec} \{mi\}) Mi_L \quad (A6)$$

For rates of change of E<sub>2</sub>17G and E<sub>2</sub>3S17G in canalicular bile (subscript, bile)

$$V_{bile} \frac{dD_{bile}}{dt} = f_L CL_{int,sec} D_L - Q_{bile} D_{bile} \quad (A7)$$

$$V_{bile} \frac{dMi_{bile}}{dt} = f_L \{mi\} CL_{int,sec} \{mi\} Mi_L - Q_{bile} Mi_{bile} \quad (A8)$$

For rates of change of E<sub>2</sub>17G and E<sub>2</sub>3S17G in collected bile samples (subscript bile,ex),

$$\frac{dA_{bile,ex}}{dt} = Q_{bile} D_{bile} \quad (A9)$$

$$\frac{dA_{bile,ex} \{mi\}}{dt} = Q_{bile} Mi_{bile} \quad (A10)$$

where  $A_{bile,ex}$  and  $A_{bile,ex} \{mi\}$  denote the cumulative secreted amount of parent drug and the formed metabolite, respectively.